THE UNIVERSITY *of* EDINBURGH

Edinburgh Research Explorer

Lateral migration of hillcrests in response to channel incision in soil-mantled landscapes

OPEN ACCESS

Lateral migration of hillcrests in response to channel incision in soil-mantled landscapes

Simon Marius Mudd

Department of Civil and Environmental Engineering, Vanderbilt University, Nashville, Tennessee, USA

David Jon Furbish

Department of Earth and Environmental Sciences and Department of Civil and Environmental Engineering, Vanderbilt University, Nashville, Tennessee, USA

[1]   We investigate lateral migration of hillcrests in response to vertical offsets or transient incision rates of channels bordering these hillcrests in soil-mantled landscapes. For hillslopes undergoing sediment transport that is linearly proportional to the slope, the hillcrest offset distance is one quarter of the ratio of the vertical offset between the channels to the relief of the symmetric hillslope. If channels are downcutting at different rates, the speed of hillcrest migration will depend on the ratio of the downcutting rates and the density ratio, which is the ratio of the bulk density of the bedrock to the bulk density of the soil. The density ratio plays a fundamental role in determining the transient response of the hillcrest; lower-density ratios lead to faster transient responses to changes in channel downcutting rates. Other parameters that affect the transient response of the hillcrest are the magnitude of transient differences in downcutting between the two channels, the time-averaged incision rate, and a ratio of the elevation of the hillslope to a length that characterizes the decay in soil production with increasing soil thickness; different parameters will be important for different sediment flux laws. The profile of soil thickness reacts to transient changes in downcutting at a different rate than surface topography. Hillslopes experiencing transient channel downcutting may have surface topography that is symmetric about the hillcrest but will at the same time have a soil thickness profile that is asymmetric.

Citation: Mudd, S. M., and D. J. Furbish (2005), Lateral migration of hillcrests in response to channel incision in soil-mantled landscapes, *J. Geophys. Res.*, *110*, F04026, doi:10.1029/2005JF000313.

1. Introduction

[2] Landscapes are dissected by drainage networks following periods of base level fall. It has been suggested [e.g., *Gilbert*, 1877; *Hack*, 1960] that after the landscape is fully dissected it will adjust to a condition in which the erosion rate averaged over the landscape will equal the rate of base level fall. There is field evidence that in areas of active tectonics, spatially averaged erosion rates equal the rock uplift rate [e.g., *Meigs et al.*, 1999; *Reneau and Dietrich*, 1991]. Field evidence also suggests that some drainage networks are stable over long periods of time in that the stream locations and profiles, and the locations of the drainage divides, do not vary significantly over time [*Bishop et al.*, 1985; *Young and McDougall*, 1993]. In some cases, however, there is evidence of drainage network change long after orogenesis. Postorogenic drainage network reorganization can occur through the migration of drainage divides [*Meyerhof*, 1972] or stream capture [*Harbor*, 1997; *Mather et al.*, 2000; *Zaprowski et al.*,

2001]. Drainage divide migration and stream capture may be due to transient changes in the rate of base level fall. Recent experimental results, however, suggest that even with a constant rate of base level fall drainage divides may migrate [*Hasbargen and Paola*, 2000]. This is in contrast to some numerical studies that have found that a constant rate of downcutting or uplift leads to stable channel and ridge networks [e.g., *Howard*, 1994; *Tucker and Bras*, 1998; *Willgoose et al.*, 1991]. *Pelletier* [2004], however, found that altering the flow routing algorithm of a landscape evolution model can lead to simulations that predict drainage divide migration, whereas *Densmore et al.* [1998] simulated migrating divides when stochastically driven landslides contributed to hillslope erosion.

[3] In their experiments, *Hasbargen and Paola* [2000] found that while the basin-averaged erosion rate may be steady the local erosion rates of subbasins may be unsteady if not cyclic. Such locally transient erosion rates can lead to the migration of drainage divides (Figure 1). Channel incision rates that vary in space and time will lead to vertical offsets of the relative elevation of adjacent channels. The hillslopes that bound the drainage divide will react to the offsets over some delayed response time if the hillslope
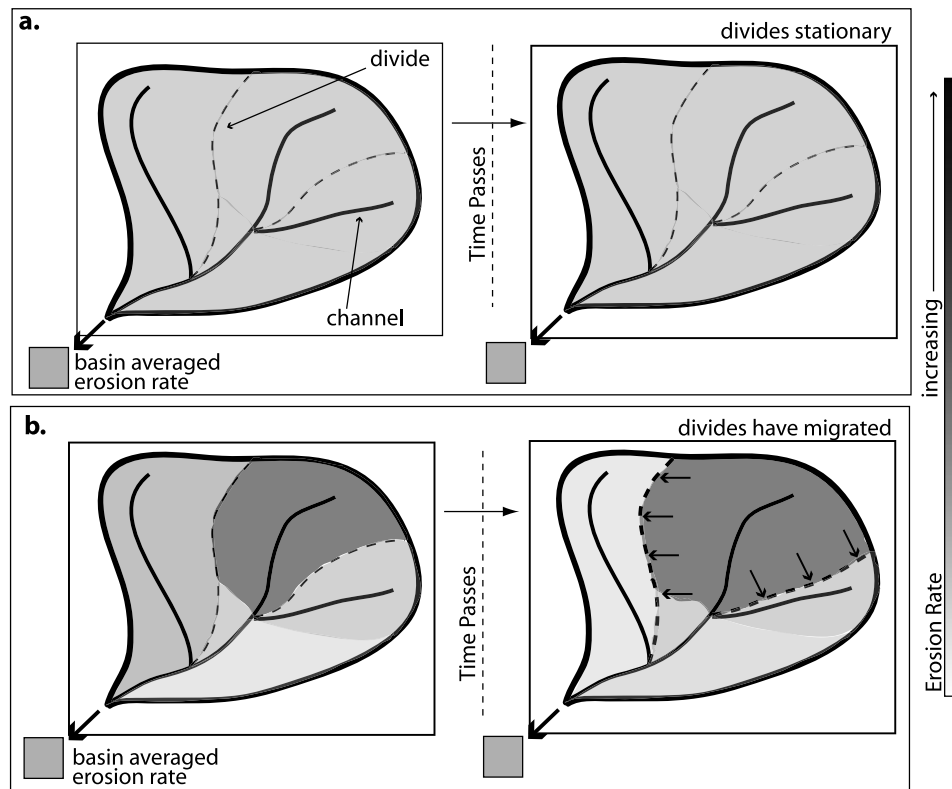
Figure 1. (a and b) Two scenarios for erosion in a basin. The basin-averaged erosion rate of both basins does not vary in time. In Figure 1a the local erosion rates equal the basin-averaged erosion rate, and the ridges are stationary. This is predicted by many numerical models for a case of constant downcutting at the basin outlet [e.g., *Howard*, 1994]. In Figure 1b, local erosion rates vary between subbasins, and divides can migrate, despite a constant rate of downcutting at the basin outlet. This has been observed in the laboratory setting [e.g., *Hasbargen and Paola*, 2000].

is undergoing creep [e.g., *Fernandes and Dietrich*, 1997; *Roering et al.*, 2001], or nearly instantaneously if the hillslopes are at a critical slope; such hillslopes will respond to base level fall with landsliding [e.g., *Burbank et al.*, 1996]. Whatever the response time, vertical offsets between adjacent channels will lead to the lateral migration of a drainage divide. If the drainage divide moves laterally, this will change the drainage area of the streams, thus changing the hydrology and sediment supply of the affected basins.

[4] Field studies in tectonically quiescent regions have reported erosion rates in adjacent streams that vary by up to a factor of two [*Kirchner et al.*, 2001; *Matmon et al.*, 2003]. Others have used stream gradients and the stream power law to estimate spatially variable stream erosion rates in tectonically active regions. *Kobor and Roering* [2004] investigated stream gradients in the Oregon Coast Range and reported that local stream downcutting rates are spatially variable, although in the Oregon Coast Range it is thought that erosion rates are in equilibrium with uplift rates over large spatial scales [*Reneau and Dietrich*, 1991]. In addition, *Finlayson et al.* [2002] found that the erosion index, a metric that combines topographic and hydrologic data used to assess potential erosion rates, varies over several orders of magnitude across the Himalaya, despite the relatively uniform convergence of the Indian subcontinent.

[5] Whereas a basin may be denuding at a constant rate averaged over geologic time, at shorter timescales stream

incision is forced by various stochastic processes [e.g., *Benda and Dunne*, 1997; *Snyder et al.*, 2003; *Tucker*, 2004]. Because the stochastic forces (such as streamflow and sediment supply) controlling incision rates in bedrock channels may be nonlinear functions of drainage area, adjacent streams that have different drainage areas may experience time histories of downcutting events that are of different magnitude and frequency, causing local disequilibrium of erosion rates. Such local disequilibrium may force the migration of drainage divides if the signal of changing incision rates can propagate up the hillslope and reach the divide. The likelihood that changes in channel downcutting rates will affect the divide in the case of a symmetric hillslope has been found to increase for variations in downcutting rates that have longer periods [*Furbish and Fagherazzi*, 2001].

[6] Here we present analytical and numerical results of our investigations of the migration of drainage divides on 1-D hillslopes (which we refer to as hillcrests) under the conditions of vertical channel offsets and transient local incision rates. First, we develop and nondimensionalize the governing equations that describe conservation of mass on a hillslope. A numerical model is then used to solve these governing equations. We use the numerical model as a virtual laboratory [e.g., *Bras et al.*, 2003] to explore the behavior of hillcrests in a number of different scenarios. These scenarios are selected to approximate natural con-
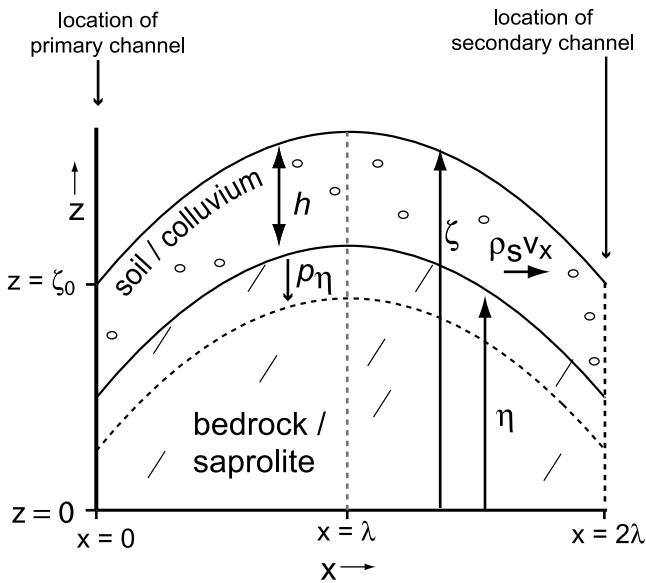
Figure 2. Schematic of the coordinate system. When incision rates in the primary and secondary are equal and constant in time, the hillcrest is at $x = \lambda$.

ditions that have been hypothesized to lead to hillcrest migration [e.g., *Hasbargen and Paola*, 2000; *Mather et al.*, 2000; *Smith and Bretherton*, 1972]. Analytical solutions are presented for specific instances of lateral hillcrest migration due to vertical channel offsets and differential channel downcutting rates. We then explore the nature of hillcrest migration on one-dimensional hillslopes that are subject to transient downcutting rates in the bounding streams, and which obey several different sediment flux laws. Two transient cases are investigated with a numerical model. The first set of model runs investigates the transient behavior of the hillcrest when knickpoints of an equal height pass through the two channels, separated by some time delay; a simplification of pulses of incision, manifested in knickpoints, that migrate through basins at different celerities [e.g., *Crosby and Whipple*, 2005]. The second set of simulations tracks the migration of the hillcrest when the time-averaged downcutting rate is the same in both channels but the instantaneous rates vary in time with different amplitudes and frequencies.

2. A 1-D Model of Hillcrest Migration

2.1. Governing Equations

[7] The basis for our hillcrest migration analysis is an equation for conservation of mass on a soil-mantled hillslope, which is depth-averaged from the soil-bedrock interface to the soil surface. In one dimension, the equation is

$$\bar{\rho}_s \frac{\partial h}{\partial t} + \bar{\rho}_s \frac{\partial (h\bar{v}_x)}{\partial x} - \rho_\eta p_\eta = 0, \tag{1}$$

where h (L) is the soil thickness, ρ_s (M L^{-3}) is the dry bulk density of the soil, v_x (L T^{-1}) is the velocity of the sediment in the x direction, ρ_η (M L^{-3}) is the density of the parent material, p_η (L T^{-1}) is the rate of bedrock lowering due to

soil production, and the overbars denote depth-averaged quantities (Figure 2). Equation (1) is a version of the equation derived by *Mudd and Furbish* [2004] that contains the assumptions that there are no sources or sinks of mass in the soil (e.g., chemical denudation) and that the depth-averaged dry bulk density is constant in time and spatially homogenous. The second assumption is reasonable for bioturbated soils, in which mechanical disturbances can loft soil to a constant porosity [*Brimhall et al.*, 1992]. We focus on hillslopes where diffusion-like sediment transport processes dominate (e.g., porous forested soils with little overland flow); we do not consider hillslopes where sediment flux due to overland flow plays a significant role.

[8] The soil thickness, h, is defined as

$$h = \zeta - \eta, \tag{2}$$

where ζ (L) is the elevation of the soil surface and η (L) is the elevation of the soil-bedrock boundary. The rate of soil production, p_η, has been found to be a function of the soil thickness,

$$p_\eta = W_0\, e^{-\frac{h}{\gamma}}, \tag{3}$$

[e.g., *Heimsath et al.*, 1999] where W_0 (L T^{-1}) is the nominal rate of soil production when the soil thickness is zero and γ (L) is a length scale that characterizes the rate of decline in the soil production rate with increasing soil thickness.

[9] Dynamic hillslope evolution is driven in part by incision at the base of the hillslope. We designate a coordinate system where the shape of the hillslope is measured relative to local base level (chosen as the elevation at the base of the hillslope):

$$\zeta_{bl} = \zeta - \zeta_0, \tag{4a}$$

$$\eta_{bl} = \eta - \zeta_0, \tag{4b}$$

where the subscript bl indicates elevation relative to base level and ζ_0 is the elevation of local base level (Figure 2). The lowering of the soil-bedrock interface relative to base level is then

$$\frac{\partial \eta_{bl}}{\partial t} = -\left(W_0 e^{-\frac{h}{\gamma}} + \frac{\partial \zeta_0}{\partial t} \right), \tag{5}$$

The second term on the right of equation (5), $\partial \zeta_0/\partial t$, is the rate of base level lowering. If the channel at the base of the hillslope is incising into bedrock, $\partial \zeta_0/\partial t$ will be negative. In the Lagrangian coordinate system, equation (1) becomes

$$\frac{\partial \zeta_{bl}}{\partial t} + \frac{\partial (h\bar{v}_x)}{\partial x} + \left(1 - \frac{\rho_\eta}{\bar{\rho}_s}\right) W_0 e^{-\frac{h}{\gamma}} + \frac{\partial \zeta_0}{\partial t} = 0. \tag{6}$$

The second term in equation (6) describes the change in surface elevation of the hillslope relative to base level due to mechanical transport processes within the soil layer. The third term is a change in surface elevation due to soil

production; it is nonzero when the dry bulk density of the soil is different from the dry bulk density of the bedrock.

[10] Mechanical sediment transport processes in the absence of overland flow can include soil creep [e.g., *Culling*, 1963; *Heimsath et al.*, 2002; *Kirkby*, 1967; *Roering et al.*, 1999; *Young*, 1978], animal burrowing and disturbance [e.g., *Gabet*, 2000], frost heave processes [e.g., *Anderson*, 2002], and tree throw and root growth [e.g., *Gabet et al.*, 2003; *Roering et al.*, 2002]. In order to close equation (6), one must use a sediment flux law [e.g., *Dietrich et al.*, 2003] to describe the sediment transport processes. A number of flux laws have been proposed and tested using field data. There is evidence that on low-relief hillslopes, sediment flux is linearly proportional to slope [*McKean et al.*, 1993; *Small et al.*, 1999]. The one dimensional linear sediment flux law can be stated as

$$h\bar{v}_x = -D\frac{\partial \zeta_{bl}}{\partial x}, \tag{7}$$

where D ($L^2\ T^{-1}$) is a sediment diffusivity. (Another coefficient occasionally reported in the literature, K, is in units of $M\ L^{-1}\ T^{-1}$ [e.g., *Fernandes and Dietrich*, 1997]. This coefficient is related to D by $K = \bar{\rho}_s D$. Some authors invert these two symbols [e.g., *Roering et al.*, 2001]; the quantities may be identified by their units). On steeper hillslopes, the interactions between disturbances, friction and gravity may lead to sediment flux that increases nonlinearly with slope [*Andrews and Bucknam*, 1987; *Roering et al.*, 1999]. This can be stated, in one dimensional form, as

$$h\bar{v}_x = -D\frac{\partial \zeta_{bl}}{\partial x}\left[1 - \left(\frac{1}{S_c}\frac{\partial \zeta_{bl}}{\partial x}\right)^2\right]^{-1} \tag{8}$$

where S_c (dimensionless) is a critical slope. We refer to equation (8) as the linear-critical flux law.

2.2. Scaling and Nondimensionalization of the Governing Equations

[11] The number of parameters in the system described by equations (5)–(8) can be reduced by nondimensionalizing the system. The variables of dimension length are non-dimensionalized with

$$\hat{x} = \frac{x}{\lambda}, \quad \hat{\zeta} = \frac{\zeta_{bl}}{\lambda}, \quad \hat{\eta} = \frac{\eta_{bl}}{\lambda}, \quad \hat{h} = \frac{h}{\gamma}, \tag{9}$$

where dimensionless quantities are denoted with carats and λ (L) is half the distance between adjacent channels (Figure 2). At both $x = 0$ and $x = 2\ \lambda$ there are channels that set the boundary condition of the hillslopes (the two hillslopes are separated by the hillcrest). We name the channel at $x = 0$ the primary channel and set its elevation to ζ_0 (the scaling of ζ_0 will be defined below). The channel at $x = 2\ \lambda$ is called the secondary channel.

[12] A length scale ratio (dimensionless) is defined as

$$\theta_L = \frac{\lambda}{\gamma}. \tag{10}$$

Note that $\hat{h} = \theta_L(\hat{\zeta} - \hat{\eta})$. A density ratio, τ_d, is defined as

$$\tau_d = \frac{\rho_\eta}{\bar{\rho}_s}. \tag{11}$$

We form a timescale defined by the parameters of the soil production function, and name this the production timescale:

$$T_P = \frac{\gamma}{W_0}. \tag{12}$$

The rate of base level lowering ($\partial\zeta_0/\partial t = I$) is scaled by

$$\hat{I} = \frac{T_P}{\gamma}\frac{\partial \zeta_0}{\partial t} = \frac{1}{W_0}\frac{\partial \zeta_0}{\partial t}. \tag{13}$$

[13] We also define a timescale based on the relaxation time of the hillslope [e.g., *Fernandes and Dietrich*, 1997; *Furbish and Fagherazzi*, 2001; *Jyotsna and Haff*, 1997]. The relaxation time is the time it takes for a hillslope to attain a new steady configuration after it has been perturbed. We define a diffusive timescale, T_D, as

$$T_D = \frac{\lambda^2}{D}. \tag{14}$$

This timescale is related to the relaxation time by a constant [e.g., *Fernandes and Dietrich*, 1997; *Furbish and Fagherazzi*, 2001; *Jyotsna and Haff*, 1997]. Time is scaled by T_D:

$$\hat{t} = \frac{t}{T_D}. \tag{15}$$

The production and diffusive timescales are used to define a timescale ratio, θ_t (dimensionless):

$$\theta_t = \frac{T_D}{T_P} = \frac{\lambda^2 W_0}{D\gamma}. \tag{16}$$

A discussion of typical timescales and timescale ratios is given by *Mudd and Furbish* [2004]. The linear and nonlinear flux laws described by equations (7) and (8) are scaled using equations (9) and (14). The resulting two equations can be written in the general form:

$$h\bar{v}_x = \frac{\lambda^2}{T_D}\phi, \tag{17}$$

where ϕ is a dimensionless function of slope with

$$\phi = \frac{\partial \hat{\zeta}}{\partial \hat{x}} \tag{18}$$

in the case of the linear sediment flux law and

$$\phi = \frac{\partial \hat{\zeta}}{\partial \hat{x}}\left[1 - \left(\frac{1}{S_c}\frac{\partial \hat{\zeta}}{\partial \hat{x}}\right)^2\right]^{-1} \tag{19}$$

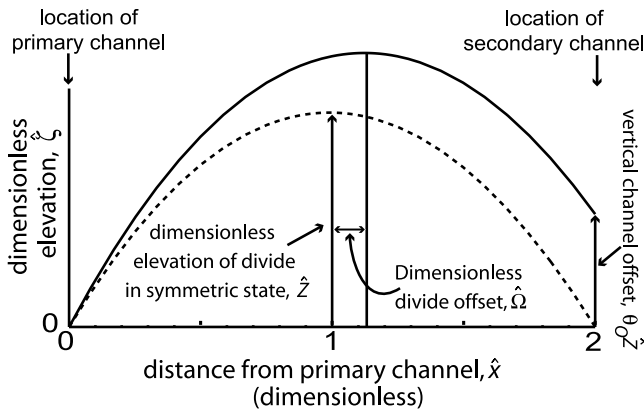in the case of the linear-critical flux law.

Figure 3. Dimensionless hillslope profiles. Dashed line is a symmetric hillslope pair, solid line shows a profile where the secondary channel is offset vertically, and the hillcrest in this profile is offset horizontally from the hillcrest of the symmetric profile.

2.3. Dimensionless Governing Equations

[14] Inserting equations (9)–(19) into equations (5) and (6) gives the nondimensionalized governing equations for the hillslope system:

$$\frac{\partial \hat{\eta}}{\partial \hat{t}} + \frac{\theta_t}{\theta_L}\left(e^{-\hat{h}} + \hat{I}\right) = 0, \tag{20}$$

$$\frac{\partial \hat{\zeta}}{\partial \hat{t}} - \frac{\partial \phi}{\partial \hat{x}} + \frac{\theta_t}{\theta_L}\left[(1-\tau_d)e^{-\hat{h}} + \hat{I}\right] = 0. \tag{21}$$

Equations (20) and (21) allow the investigation, through both analytic and numerical techniques, of scenarios that will lead to hillcrest migration.

3. Analytical Solutions of Hillcrest Migration

[15] Analytical solutions can be obtained for specific cases of hillcrest migration. We solve equations (20) and (21) for two cases: in the first case the channels are incising at the same rate but are offset vertically, and in the second case the adjacent channels are incising at constant but different rates.

3.1. Hillcrest Offset Due to Channel Elevation Differences at Topographic Steady State

[16] Consider a one-dimensional hillslope between two channels that is at topographic steady state relative to local base level ($\partial\hat{\zeta}/\partial\hat{t} = \partial\hat{\eta}/\hat{t} = 0$). The steady state condition implies that the production rate of soil is spatially uniform. If the channels that bound the ridge are at the same elevation, the hillslopes on either side of the ridge will be symmetric. If, however, the channels are at different elevations, the hillcrest will be offset toward the channel at a higher elevation. In this section we determine how the offset distance is affected by the dominant sediment flux law, the characteristics of the hillslope (e.g., hillslope relief) and the vertical offset of the two channels bounding the hillslope.

[17] The horizontal offset of the hillcrest can be found analytically by solving equations (20) and (21) simplified for topographic steady state. Setting the time derivative in

equation (20) to zero yields $\exp(\hat{h}) = -\hat{I}$. We assume sediment transport is linearly proportional to the slope (equations 7, 17 and 18) and set the time derivative in equation (21) to zero, giving an equation for the curvature of the hillslope:

$$\frac{\partial^2 \hat{\zeta}}{\partial \hat{x}^2} = \frac{\theta_t}{\theta_L}\tau_d\hat{I}. \tag{22}$$

The surface topography may be found by integrating equation (22) twice and applying the appropriate boundary conditions. The dimensionless surface elevation is set to zero at $\hat{x} = 0$. At $\hat{x} = 2$, which is the location of the secondary channel, the surface elevation is offset from the elevation of the channel at $\hat{x} = 0$. This vertical offset is measured as a fraction of the elevation of the hillcrest if both channels were incising at the same rate. The elevation at the hillcrest for a steady state hillslope when both channels are at the same elevation ($\hat{Z}_{ls}$, dimensionless) is

$$\hat{Z}_{ls} = -\frac{\tau_d\theta_t}{2\theta_L}\hat{I}. \tag{23}$$

The offset ratio, θ_O, is defined as

$$\hat{\zeta}|_{\hat{x}=2} = \theta_O\hat{Z}_{ls} \tag{24}$$

where $\hat{\zeta}|_{\hat{x}=2}$ is the dimensionless elevation of the secondary channel (see Figure 3). Using equations (23) and (24) as the second boundary condition for equation (22), the hillslope profile may be found:

$$\hat{\zeta} = \frac{\tau_d\theta_t}{\theta_L}\hat{I}\left[\frac{\hat{x}^2}{2} - \left(\frac{\theta_O}{4} + 1\right)\hat{x}\right]. \tag{25}$$

The hillcrest offset, $\hat{\Omega}$ (dimensionless), is measured as the distance from $\hat{x} = 1$ (see Figure 3) and may be found by setting the slope of equation (25) to zero, solving for $\hat{x}$, and subtracting one:

$$\hat{\Omega} = \frac{\theta_O}{4}. \tag{26}$$

Equation (26) demonstrates that the hillcrest offset in the case of the linear sediment flux law is a simple function of geometry. That is, the hillcrest offset is one quarter of the offset ratio.

[18] For comparison, we can calculate the hillcrest offset distance for the case of rapidly incising, steep topography. *Burbank et al.* [1996] found that in the Himalaya in a region of rapid incision, slope angles were independent of the incision rate, suggesting that a threshold slope had been attained. Imagine two rivers separated by hillslopes at a threshold slope, S_T (this slope was found to be ~0.8 [*Burbank et al.*, 1996]). The dimensionless elevation of the hillcrest when both channels are at the same elevation is simply S_T, and if the river is offset by the product of θ_O and S_T, the hillcrest offset distance will be

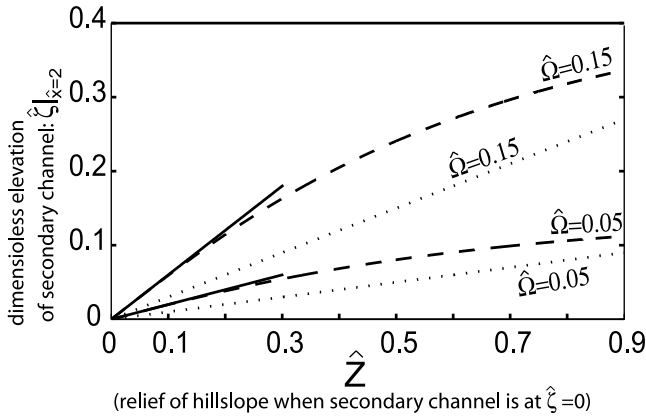$$\hat{\Omega} = \frac{\theta_O}{2}. \tag{27}$$

Figure 4. Contours of the dimensionless hillcrest offset ($\hat{\Omega}$) as a function of hillslope relief and vertical channel offset. The solid line is for hillslopes experiencing a linear sediment flux law, the dashed line is for linear-critical slopes, and the dotted line is for threshold slopes.

Recall that the linear sediment flux law applies to landscapes with gentle slopes. These two cases can be thought of as end member scenarios. In landscapes where slopes are gentle and incision rates are lower, vertical offsets in the elevations of adjacent channels will move the hillcrest a quarter of the offset ratio according to equation (26), whereas in rapidly eroding landscapes a vertical channel offset can cause twice the hillcrest offset as a fraction of the relief of the symmetric hillslope.

[19] It should be noted, however, that landscapes where rivers are bounded by critical hillslope are generally high-relief landscapes, such as the Himalaya [e.g., *Burbank et al.*, 1996]. Suppose a knickpoint of some arbitrary height is generated due to a faulting or rapid sea level change. This knickpoint then migrates through a lower-relief, soil-mantled foreland and subsequently into a high-relief mountainous area which has hillslopes at a threshold angle. In such a case the knickpoint would be a much smaller fraction of the relief in the high-relief mountainous region than in the lower-relief, soil-mantled region. The ratio of the dimensional hillcrest offset distances in such a case is

$$\frac{\Omega_{ts}}{\Omega_{lr}} = -\frac{\lambda_{ts}\tau_d}{DS_T}\frac{\partial\zeta_0}{\partial t}, \qquad (28)$$

where the subscript *ts* denotes the high-relief, threshold slope landscape and the diffusivity, base level lowering rate, and bedrock to soil density ratio are all measured in the soil-mantled landscape where sediment transport follows equation (18).

[20] As an example, consider a knickpoint that is 10 m in height (the 1996 Chichi earthquake in Taiwan had a vertical offset of 3–8 m [*Chen et al.*, 2002]) that is generated on a landscape which has a background base level lowering rate of 0.01 mm yr^{-1} in the foreland area. Suppose that in the hillslopes throughout this landscape are on average 500 m long, there is no density contrast between the soil and the bedrock, the diffusivity in the soil-mantled foreland is 0.025 m^2 yr^{-1}, and the threshold slope is 0.8 in the mountainous area. Note that the base level lowering rate

could be significantly higher in the mountainous area compared to the foreland area; background base level lowering plays no role in the amount of relief in landscapes with hillslopes at a threshold angle. Under these conditions, the knickpoint would cause the hillcrest in the foreland area to be offset by 25 m, whereas the offset in the mountainous, threshold portion of the landscape from this same knickpoint would be 6.25 m.

[21] We may also compare the behavior of the above instances with the case of a hillslope where sediment transport follows a linear-critical sediment flux law (equation (8)). The profile of a hillslope experiencing linear-critical sediment transport at steady state is described by:

$$\hat{\zeta} = S_c\sqrt{\frac{S_c^2}{16\hat{Z}_{ls}^2} + \hat{X}^2} - S_c\sqrt{\frac{S_c^2}{16\hat{Z}_{ls}^2} + (\hat{x} - \hat{X})^2}$$

$$+ \frac{S_c^2}{4\hat{Z}_{ls}}\ln\left[1 + \sqrt{1 + \frac{16(\hat{x} - \hat{X})^2\hat{Z}_{ls}^2}{S_c^2}}\right]$$

$$- \frac{S_c^2}{4\hat{Z}_{ls}}\ln\left[1 + \sqrt{1 + \frac{16\hat{X}^2\hat{Z}_{ls}^2}{S_c^2}}\right], \qquad (29)$$

where $\hat{X}$ (dimensionless) is the location of the hillcrest. The symmetric case, where there is no hillcrest offset, is found by setting $\hat{X}$ to one. We may solve for the elevation at the secondary channel by setting $\hat{x}$ to two. This leads to a transient (nonalgebraic) equation in $\hat{X}$; an analytic solution of the hillcrest offset as a function of S_c, $\hat{Z}_{ls}$, and θ_O has not been found. We may solve for the vertical channel offset for various values of the hillcrest offset and the elevation of the hillcrest in the symmetric case and compare these offsets with the linear and critical hillslope cases. Figure 4 plots contours of the dimensionless hillcrest offset ($\hat{\Omega}$) as functions of the relief of the hillslope when it is in symmetric state ($\hat{Z}$) and the elevation of the secondary channel (recall the primary channel is always at an elevation of $\hat{\zeta} = 0$). We have plotted the hillcrest offset as a function of the relief of the hillslopes in the symmetric state because it is not a function of the elevation of the secondary channel. For low-relief hillslopes (low values of $\hat{Z}$), the behavior of the hillslopes obeying a linear-critical flux law approaches the behavior of the hillslopes obeying the linear sediment flux law. As the relief of the hillslopes increase, the linear-critical slopes behave more like the threshold slopes. If two hillslopes experience a vertical offset of the same dimensionless height, the hillslope with less relief will experience the greater hillcrest offset. For hillslopes with the same vertical offset and the same relief, the hillcrest offset will be greatest for the threshold slopes, followed by the linear-critical slopes, with the hillslopes where sediment flux goes linearly with slope having the lowest hillcrest offset.

3.2. Migrating Hillcrest Due to Steady But Unequal Channel Incision Rates

[22] To examine the possibility of stream capture associated with hillcrest migration, we consider the case in which two adjacent channels are incising at steady, but different, rates. The incision rate of the channel at $\hat{x} = 0$ is $\hat{I}$, and at
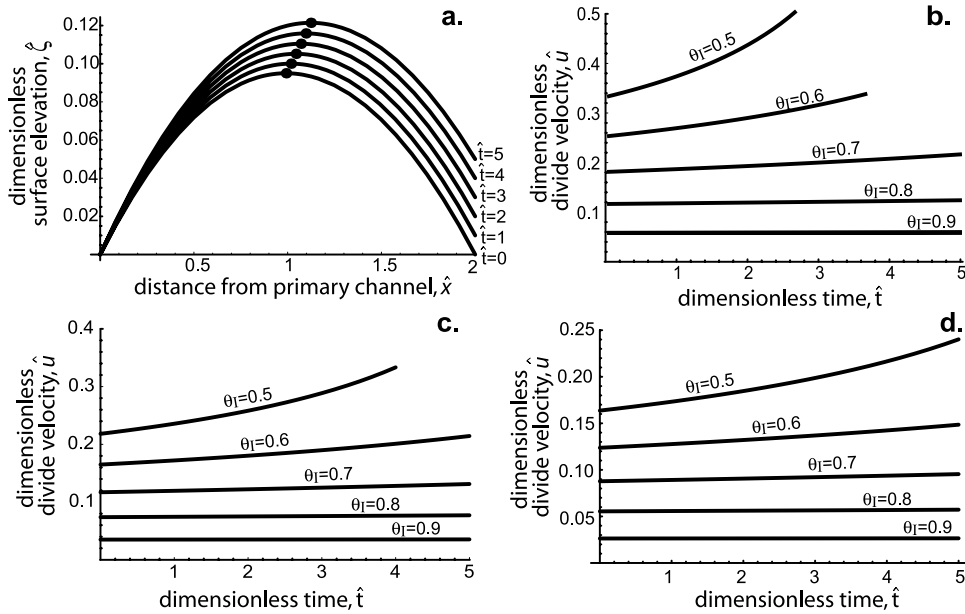
Figure 5. Pseudo steady state hillcrest migration. The parameter θ_I is the ratio of the rate of incision in the secondary channel to the rate of incision in the primary channel. (a) Profile of a hillslope where the secondary channel is incising at a slower rate than the primary channel. Dots denote the location of the hillcrest. Parameters are $\tau_d = 2$, $\theta_t = 10$, $\theta_D = 100$, $\hat{I} = -0.1$, and $\theta_I = 0.9$. (b) Dimensionless velocity of the hillcrest for $\tau_d = 1$. (c) Dimensionless velocity of the hillcrest for $\tau_d = 1.5$. (d) Dimensionless velocity of the hillcrest for $\tau_d = 2$. In Figure 5b, for $\theta_I = 0.5$, $\theta_I = 0.6$ and in Figure 5c for $\theta_I = 0.5$ the plots end where the location of the hillcrest is $\hat{x} = 2$. Note the change in vertical scale in Figures 5b and 5c.

$\hat{x} = 2$ the incision rate is set to a fraction of $\hat{I}$, which we call θ_I (dimensionless). If the channel at $\hat{x} = 2$ is incising at a different rate than the channel at $\hat{x} = 0$, then the relative elevation of the channel at $\hat{x} = 2$ will change:

$$\left.\frac{\partial \hat{\zeta}}{\partial \hat{t}}\right|_{\hat{x}=2} = \frac{\theta_t}{\theta_L}\hat{I}(\theta_I - 1). \qquad (30)$$

Numerical solutions have demonstrated that from arbitrary initial conditions and steady but unequal downcutting rates at $\hat{x} = 0$ and $\hat{x} = 2$, the soil thickness reaches a steady state after some finite period of time ($\partial \hat{h}/\partial t = 0$). We call this a pseudo steady state because while the soil thickness does not change in time, the surface topography is transient, and the pseudo steady state condition only exists until the channel that is incising at a slower rate is captured by the fast eroding channel. When the dimensionless soil production rate, $\exp(-\hat{h})$, reaches its steady state condition it is a linear function of $\hat{x}$. This linear function is:

$$e^{-\hat{h}} = \frac{\hat{I}(1 - \theta_I)}{2}\hat{x} - \hat{I}. \qquad (31)$$

Equation (31), combined with the dimensionless equation for soil thickness using the linear flux law, results in an equation for the curvature of the pseudo steady state hillslope:

$$\frac{\partial^2 \hat{\zeta}}{\partial \hat{x}^2} = \frac{\theta_t \tau_d}{\theta_L}\hat{I} - \frac{\theta_t \tau_d}{\theta_L}\frac{\hat{I}(1 - \theta_I)}{2}\hat{x}. \qquad (32)$$

At $\hat{x} = 0$, the boundary condition is $\hat{\zeta} = 0$. At $\hat{x} = 2$, the boundary condition may be found by integrating with respect to time and letting $\hat{\zeta}$ at $\hat{t} = 0$ be equal to zero:

$$\hat{\zeta}|_{\hat{x}=2} = \frac{\theta_t}{\theta_L}\hat{I}(\theta_I - 1)\hat{t}. \qquad (33)$$

These two boundary conditions may be used to solve for the pseudo steady state topography:

$$\hat{\zeta} = -\frac{\tau_d \theta_t \hat{I}(1 - \theta_I)}{12\theta_L}\hat{x}^3 + \frac{\tau_d \theta_t \hat{I}}{2\theta_L}\hat{x}^2$$
$$+ \frac{\theta_t \hat{I}}{2\theta_L}(1 - \theta_I)\hat{t}\hat{x} - \left(\frac{\tau_d \theta_t \hat{I}}{\theta_L} - \frac{\tau_d \theta_t \hat{I}[1 - \theta_I]}{3\theta_L}\right)\hat{x}. \qquad (34)$$

The dimensionless elevation of the hillslope ($\hat{\zeta}$) is a function of both $\hat{x}$ and $\hat{t}$. The hillcrest is located where the slope of the soil surface equals zero. The location of the hillcrest, $\hat{x}_d$, is found to be:

$$\hat{x}_d = \frac{\sqrt{6\tau_d\left(2\tau_d + 2\theta_I[3\hat{t} + \tau_d] + \theta_I^2[2\tau_d - 3\hat{t}] - 3\hat{t}\right)} - 6\tau_d}{3(\theta_I - 1)\tau_d}. \qquad (35)$$

The dimensionless lateral migration speed of the hillcrest, $\hat{u}_d$, is found by differentiating equation (35) with respect to dimensionless time:

$$\hat{u}_d = \frac{3(1 - \theta_I)}{\sqrt{6\tau_d\left(2\tau_d - 3\hat{t} + 2\theta_I[3\hat{t} + \tau_d] + \theta_I^2[2\tau_d - 3\hat{t}]\right)}}. \qquad (36)$$
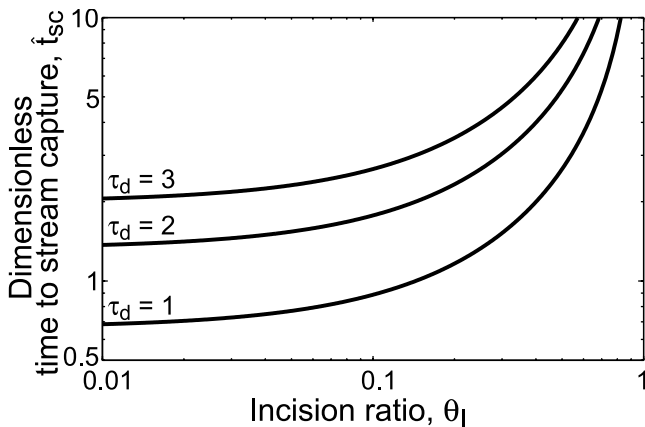
Figure 6. Dimensionless time to stream capture ($\hat{t}_{sc}$) as a function of the incision ratio θ_I and the density ratio τ_d. As θ_I approaches 1, $\hat{t}_{sc}$ asymptotically approaches infinity.

The dimensionless incision rate ($\hat{I}$) of the primary channel and the time and length ratios (θ_t and θ_D) are important in determining the curvature, slope, and relief of the pseudo steady state hillslope, but they play no role in determining the location and migration speed of the hillcrest. The behavior of the hillcrest is solely a function of θ_I, τ_d, and $\hat{t}$. Figure 5 shows some of the behavior of the pseudo steady state hillslope. As the secondary channel incises at a slower rate than the primary channel, the relative elevation of the secondary channel increases, and the hillcrest migrates away from the primary channel (Figure 5a). In all cases the migration speed of the hillcrest increases with time. As θ_I approaches one, the relationship between $\hat{u}_d$ and $\hat{t}$ may be approximated as linear, but at smaller values of θ_I (when the secondary channel is being offset from the primary channel at a faster rate), $\hat{u}_d$ increases nonlinearly with time (Figures 5b–5d). The density ratio (τ_d) is inversely related to $\hat{u}_d$ (equation 36), and $\hat{u}_d$ also decreases with increasing θ_I. Lower values of θ_I mean that the vertical offset distance between channels will increase more rapidly (equation 34), and the faster this relief between channels is generated, the faster the hillcrest migrates.

[23] Stream capture occurs when the location of the hillcrest equals the location of the secondary channel ($\hat{x}_d = 2$). The dimensionless time to stream capture ($\hat{t}_{sc}$) is found by setting the hillcrest location equal to the location of the secondary channel in equation (35) and solving for time:

$$\hat{t}_{sc} = -\frac{2\tau_d(1 + 2\theta_I)}{3(\theta_I - 1)} \qquad (37)$$

Figure 6 shows how $\hat{t}_{sc}$ varies with variations in θ_I. For small values of θ_I, meaning that the vertical offset elevation between the primary and secondary channel grows rapidly, $\hat{t}_{sc}$ can approach or be less than one (the time to stream capture approaches the relaxation time of the hillslope). As θ_I moves to values of $0.3–0.4$, the time to stream capture begins to increase rapidly, and as θ_I approaches one the time to stream capture approaches infinity.

[24] Both *Matmon et al.* [2003] and *Kirchner et al.* [2001] have measured θ_I values approaching 0.5 in the field (see Table 1). In the drainage basins measured for these two studies, the channel spacing is large enough ($O(10^3–10^4 \text{ m})$) that the imbalance in erosion rates over adjacent basins would need to persist for tens of millions of years for a basin to capture the adjacent stream via this mechanism. For example, with $\lambda = 500$ m (the approximate spacing between basins one and two in the work by *Kirchner et al.* [2001]), $D = 0.025 \text{ m}^2 \text{ yr}^{-1}$, no density difference between the soil and bedrock ($\tau_d = 1$), and $\theta_I = 0.5$, the time to stream capture from a symmetrical state (the two channels are at the same elevation) would be 2.66×10^7 years. The hillcrest migration speed in such a case would be on the order of 0.01 mm yr^{-1}. This rate may seem negligible, but consider a situation in which $\lambda = 100$ m, a scale at which the basin-averaged erosion rates in adjacent basins have yet to be measured using detrital cosmogenic radionuclides. With all other parameters the same as above excluding the channel spacing, the time to stream capture decreases to $\sim 1 \times 10^6$ years. This time would reduce to five hundred thousand years if θ_I were 0.2, which is the ratio of erosion rates between adjacent catchments reported by *Riebe et al.* [2000] at Fort Sage, California. The cosmogenic isotope method used to calculate the spatially varying erosion rates by both *Matmon et al.* [2003] and *Kirchner et al.* [2001] averages rates over this timescale; such a duration of an average imbalance in erosion rates between adjacent basins is reasonable. To dimensionalize the hillcrest migration velocity, the dimensionless velocity is multiplied by the factor λ/D, so shorter slopes with higher diffusivities will have faster hillcrest migration velocities. More field studies quantifying spatially varying rates of erosion in adjacent basins at the $\lambda \leq 100$ m scale could better constrain the likelihood of stream capture through a mechanism of differential downcutting rates in adjacent basins.

[25] Consider also the problem of escarpment retreat. A number of authors have suggested that escarpments can retreat at rates of 1 mm yr^{-1} if the escarpment has retreated at a constant rate since the time of rifting, whereas others have suggested that the recent retreat rates are considerably slower, and that a majority of the retreat occurred shortly after rifting (for an overview, see *van der Beek et al.* [2002] and references therein). On the southeastern Australian escarpment *Heimsath et al.* [2000] found that on the coastal side of the escarpment the basin-averaged erosion rate (measured using [10]Be concentration in river sand) was

Table 1. Measured Incision Ratios of Adjacent Basins[a]

Basin Reference	θ_I	Source
25,27	0.68 ± 0.18	1
26,27	0.69 ± 0.19	1
14,15	0.71 ± 0.21	1
1,2	0.55 ± 0.14	1
GSCS-1, GSCS-2	0.49 ± 0.12	2
GSBC-1, GSCA-1	0.59 ± 0.15	2
GSCO-4, GSRF-11	0.57 ± 0.14	2
Fall River	0.50 ± 0.11	3
Fort Sage	0.16 ± 0.07	3

[a]Basin reference are the location names used by *Kirchner et al.* [2001] (source 1), *Matmon et al.* [2003] (source 2), and *Riebe et al.* [2000] (source 3) of the adjacent basins used to calculate θ_I. The data from *Riebe et al.* [2000] were derived from their Figure 1.
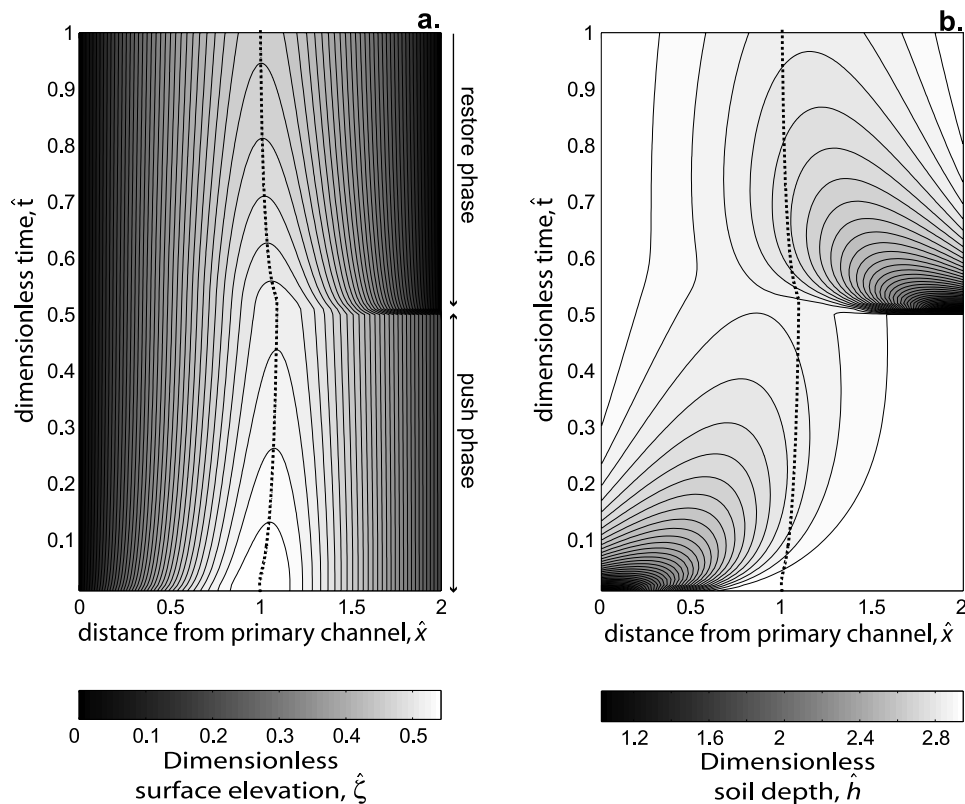
Figure 7. (a and b) Transient behavior of a hillslope subjected to two knickpoints of the same elevation. Plots are read from bottom to top for advancing dimensionless time ($\hat{t}$); a horizontal slice through Figures 7a and 7b would represent a profile at a given $\hat{t}$. In Figure 7a, contours represent surface elevation. In Figure 7b, contours represent soil thickness The dotted lines in Figures 7a and 7b show the location of the hillcrest.

51.49×10^{-6} m yr^{-1}, whereas the basin-averaged erosion rate on the upland side of the escarpment was 15.47×10^{-6} m yr^{-1}. This difference in erosion rates could lead to migration of the hillcrest, contributing to escarpment retreat; the difference in erosion rates gives a θ_I value of 0.3 between the coastal and upland side of the escarpment. *Heimsath et al.* [2001] also found the diffusivity to be 0.004 m^2 yr^{-1}. We consider the hillslope length in this case the distance from the hillcrest to the channel head. For hillslopes with lengths on the order of 10–100 m and with a density ratio (τ_d) of 1.5, the hillcrest retreat rates would be on the order of 10^{-4} to 10^{-5} m per year. This should be considered only a rough estimate of escarpment retreat rates due to the fact that as the hillslope on the fast eroding side of the escarpment grows in length as the hillcrest migrates toward the upland, the location of the fluvial network is likely to change.

[26] For hillcrests that migrate rapidly, the diffusivities would have to be extremely high, the hillslopes short, density differences between soil and bedrock low, and the difference in erosion rates on either side of the escarpment pronounced. For example, with no difference in the densities of soil and bedrock ($\tau_d = 1$), hillslopes that are 20 m long, a difference in erosion rates of a factor of 20 ($\theta_I = 0.05$), and a diffusivity at the upper range of any measured ($D = 0.03$ m^2 yr^{-1}; see *Fernandes and Dietrich* [1997] for a

range of diffusivities) the hillcrest would migrate at a rate on the order of 1 mm per year.

4. Numerical Simulations of Transient Hillcrest Migration

[27] To investigate the transient response of the hillslope hillcrest to unsteady downcutting in the primary and secondary channels we solve equations (20) and (21) numerically. We focus the numerical investigation on two scenarios of transient channel incision. The first scenario models knickpoints propagating through a drainage basin. Two knickpoints of identical elevation travel through the primary and secondary channel, but there is a delay between the time these knickpoints pass the base of the hillslope. This delay is a natural feature of knickpoint propagation because the celerity of the knickpoint varies between basins if they have different sediment supplies or water discharges [*Crosby and Whipple*, 2005; *Whipple and Tucker*, 1999]. The second scenario models the effect of having incision rates that vary with different frequency and amplitude in the primary and secondary channels. This variation is an approximation of downcutting of streams that have different thresholds for channel incision and flood distributions that cause temporal variations in downcutting rates [e.g., *Snyder et al.*, 2003; *Tucker*, 2004]. For these two cases, the long-

term average erosion rate is set to be the same in both the primary and secondary channel.

4.1. Effect of Delayed Knickpoint Migration

[28] In the first set of simulations the two channels bounding a 1-D hillslope pair are incising at a background rate $\hat{I}$. A knickpoint passes through the primary channel at $\hat{t} = 0$. It incises a fraction of the total relief of the hillslope θ_{kp}. After a delay time of $\hat{t}_{kpd}$, a knickpoint of the same elevation passes through the secondary channel. A finite difference model is used to track the transient response of the hillslopes separating the channels to the passage of these knickpoints. The response of a hillslope with a linear flux law (equation (7)) has been explored by *Fernandes and Dietrich* [1997] and *Roering et al.* [2001], but the simulations presented here differ in both the forcing (in the form of incision rates) and the incorporation of soil production. Additionally we allow asymmetry of the hillslope, which leads to hillcrest migration.

[29] Inclusion of soil production in modeling the transient response of a hillslope is significant in two important ways. First, as will be shown later in this section, the expansion (or contraction) of the material on the hillslope as it is converted from bedrock to soil (encapsulated in the parameter τ_d) acts as a first-order control on the transient response of the hillslope. Second, the response of the soil thickness can lag behind the response of the surface topography.

4.1.1. Linear Flux Law

[30] In the first set of delayed knickpoint migration simulations, a linear sediment flux law is used (equation (7)). When a knickpoint in the primary channel reaches the base of the modeled hillslope, the hillslope is steepened near the channel and responds with increased sediment flux. The increased sediment flux from the disturbance causes soil to be evacuated (Figure 7). Evacuation of soil causes a reduction in the soil thickness, thus causing an increase in soil production (see equation 3). After the initial wave of increased sediment flux and the corresponding decrease in soil thickness, the soil recovers back to its steady thickness, but at a rate different from the rate of return to steady surface topography. Figure 7a shows the response of the surface topography to the passage of the two knickpoints, and Figure 7b shows the response of the soil thickness. After the passage of each knickpoint the disturbances in soil thickness move away from the disturbed channel, widen, and decay (Figure 7b). The disturbance to the surface topography propagates upslope until it reaches the hillcrest, at which point it begins to "push" the hillcrest away from the disturbed channel. As the disturbance in topography and soil depth moves away from the primary channel and approaches the hillcrest, soil is evacuated toward the disturbed channel, and the sediment flux toward the undisturbed channel is reduced. This reduces the soil depth downslope of the hillcrest away from the disturbed channel. We call the period during which the hillcrest moves away from the primary channel the push phase. As the hillcrest moves toward the secondary channel a wave of increased erosion propagates away from the secondary channel. At some time after the second channel has been disturbed the hillcrest begins to migrate back toward its equilibrium position at $\hat{x} = 1$. We refer the period of time between the time the hillcrest begins to migrate back toward the primary channel due to the passage of the second knickpoint and the time when the hillcrest returns to the equilibrium position the restore phase.

[31] The motion of the hillcrest has a characteristic shape (e.g., the dotted lines in Figure 7) determined by the processes described in the previous section. Numerical simulations have shown this motion to be a function of the knickpoint delay $\hat{t}_{kpd}$, the density ratio τ_d, the knickpoint ratio θ_{kp}, and a ratio θ_Z:

$$\theta_Z = \frac{1}{2} \frac{\lambda^2}{D\gamma} \frac{\partial \zeta_0}{\partial t}. \tag{38}$$

The quantity θ_Z is the ratio between the time it takes soil eroding at the background rate $\partial \zeta_0 / \partial t$ to erode through soil of thickness 2γ and the relaxation time of the hillslope. For example, a hillslope with a background incision rate of 2.5×10^{-5} m yr^{-1} (similar to the erosion rates measured with ^{10}Be in the Smokey Mountains [*Matmon et al.*, 2003] and southeast Australia [*Heimsath et al.*, 2001]), a soil production length scale (γ) of 0.5 m, a diffusivity of 0.01 m^2 yr^{-1}, and a hillslope length (λ) of 100 m would have a θ_Z value of 25.

[32] At an approximation, both the push phase and the restore phase may be described by an exponential decay function of the form:

$$F(\hat{t}) = F_e + (F_s - F_e)e^{-\frac{\hat{t}}{\kappa}}, \tag{39}$$

[e.g., *Howard*, 1988; *Roering et al.*, 2001] where $F(t)$ is some function of time (in this case the location of the hillcrest) F_s is the value of the function at the start time (and perturbed from equilibrium), and F_e is the value at the function at equilibrium. In the case of the push phase F_e is the theoretical maximum push distance (equation (26)) and in the case of the restore phase F_e is $\hat{x} = 1$. The decay constant, κ, is a dimensionless parameter that determines how quickly the system will adjust to perturbations. It is a response time that is scaled, like $\hat{t}$, by the relaxation time of the hillslope. The decay constant, κ, represents the time it takes the hillcrest to respond to perturbation as a fraction of the hillslope relaxation time. For example, if $\kappa = 0.1$, the disturbed hillcrest will have migrated ninety percent of the distance to the maximum theoretical offset after a period of 0.23 times the hillslope diffusive timescale ($T_D = \lambda^2/D$), whereas if $\kappa = 1$ the hillcrest will have migrated back to a tenth of the original disturbance after period of 2.3 times T_D.

[33] In some cases, the exponential approximation may be relatively poor. Closer examination of the motion of the hillcrest reveals that the exponential fit of the hillcrest relaxation time varies in dimensionless time. To illustrate this more complex behavior, we linearize equation (39) with respect to $\hat{t}$:

$$X = \frac{\hat{t}}{\kappa}, \tag{40a}$$

where

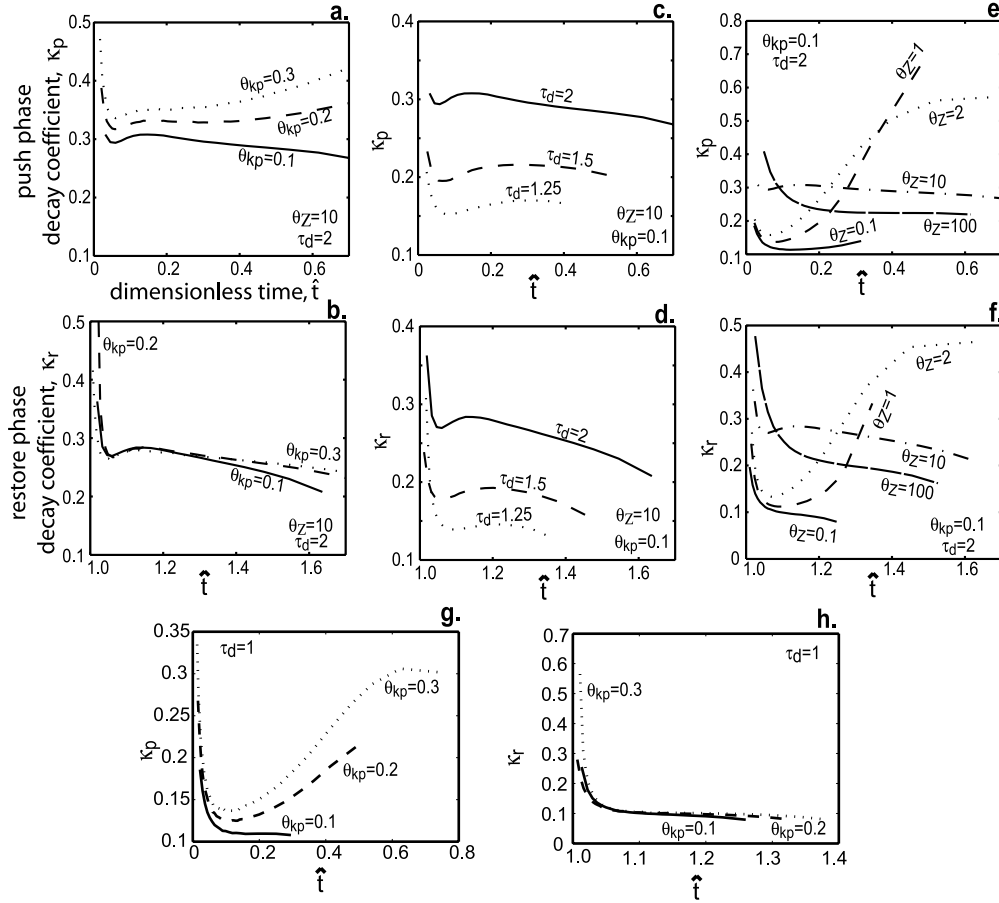$$X = -\ln\left[\frac{F(\hat{t}) - F_e}{F_s - F_e}\right]. \tag{40b}$$

Figure 8. Relaxation time of hillcrest migration as a fraction of hillslope relaxation time (κ). All runs have a $\hat{t}_{kpd}$ of 1. Figures 8a and 8b show variation in θ_{kp} with other parameters held constant for (a) push and (b) restore phases. Figures 8c and 8d show variation in τ_d with other parameters held constant for (c) push and (d) restore phases. Figures 8e and 8f show variation in θ_Z with other parameters held constant for (e) push and (f) restore phases. Figures 8g and 8h show variation in θ_{kp} with $\tau_d = 1$ for (g) push and (h) restore phases. In Figures 8g and 8h, there is no sensitivity to θ_Z. Note the change in vertical scale.

The slope of the line that defines X as a function of $\hat{t}$ is related to the hillcrest relaxation time as a fraction of the hillslope relaxation time:

$$\frac{dX}{d\hat{t}} = \frac{1}{\kappa}. \qquad (41)$$

We define two decay coefficients, $\kappa_p(\hat{t})$ for the push phase and $\kappa_d(\hat{t})$ for the restore phase. This approach allows us to examine the adjustment rate of the hillcrest as a function of time. This approach is necessary because the hillslope-soil system is responding on two different timescales which lead to a complex response of the system to transient perturbations. The two timescales are related to the adjustment of topography from sediment fluxes (which respond to changes in slope), and the adjustment of soil production (which respond to changes in soil depth). A time varying κ measures the changing rate of adjustment of the hillcrest to the equilibrium state as the coupled system responds to transient changes in channel incision rates. Greater hillcrest relaxation times (e.g., greater κ values) represent slower adjustment of the hillcrest to channel perturbations, whereas smaller hillcrest relaxation times (e.g., smaller κ values)

represent faster adjustment of the hillcrest to channel perturbations.

[34] Variations in the density ratio τ_d and the offset ratio θ_{kp} lead to systematic variations in the hillcrest relaxation time throughout the duration of the push phase. Increasing θ_{kp} leads to increasing hillcrest relaxation times in both the push and restore phases (κ_p and κ_r, e.g., Figure 8a). Increasing θ_{kp} increases the disturbance of the surface topography relative to the relief of the hillslope, which would presumably lead to faster response times, but the hillcrest also must move farther from equilibrium, increasing the response time. The numerical results imply that the increased distance the hillcrest must migrate to reach equilibrium is more significant in determining the adjustment rate than the perturbation in surface topography caused by the knickpoint.

[35] Increasing τ_d (greater soil lofting) increases the relaxation time of the hillcrest (Figures 8c and 8d), except in some cases shortly after the passage of the second knickpoint (Figure 8d). The relaxation time of the hillcrest is more sensitive to changes in τ_d than to changes in θ_{kp} early in the push phase and throughout the restore phase (compare Figure 8a to Figure 8c and Figure 8b to Figure 8d).
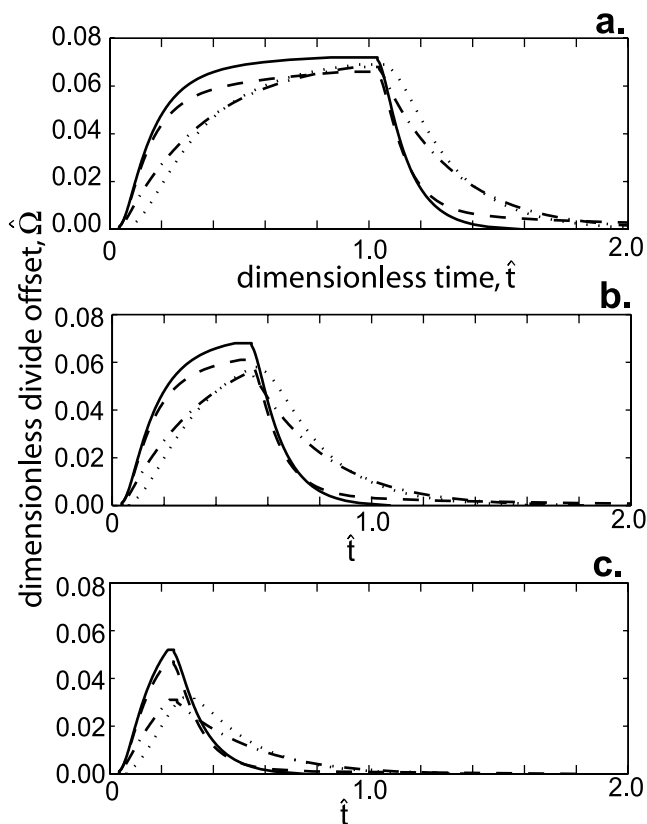
Figure 9. Hillcrest offset through dimensionless time for hillslopes with linear sediment transport, $\tau_d = 2$, and $\theta_{kp} = 0.3$: (a) $\hat{t}_{kpd} = 1$, (b) $\hat{t}_{kpd} = 0.5$, and (c) $\hat{t}_{kpd} = 0.2$. The solid lines have $\theta_Z = 0.1$, the dashed lines have $\theta_Z = 1.0$, the dash-dotted lines have $\theta_Z = 10$, and the dotted lines have $\theta_Z = 100$.

For example, consider a hillslope with a diffusivity (D) of 0.02 m^2 yr^{-1} and a length (λ) of 40 m, and all other parameters the same as those used to generate Figure 8b. The diffusive timescale of this hillslope is then 80 ka. Such a hillslope whose soil is half as dense as the bedrock ($\tau_d = 2$) will have its hillcrest migrate ninety percent of the distance to its maximum theoretical offset (determined by equation 26) within approximately 50 ka. If the soil is density ratio is lowered to 1.25, however, this time becomes approximately 30 ka.

[36] The relaxation time of hillcrest migration responds in a complex way to changes in θ_Z (Figures 8e and 8f). When the disturbance caused by a knickpoint first reaches the hillcrest the rate of response is greater for hillslopes with smaller values of θ_Z (with smaller values of κ corresponding to faster response rates, Figures 8e and 8f). As time passes however, the response rates adjust, and for larger values of time the response rate increases with increasing values of θ_Z. The physics of this complex response can be further elucidated by examining the special case of $\tau_d = 1$. Examination of equation (21) reveals that if $\tau_d = 1$, then the first term in the brackets goes to zero. This term is the transient response of the surface due to the lofting of the soil as it is converted from its parent material. When $\tau_d = 1$, the response of the hillcrest has no dependance on θ_Z. The changes in the relaxation time of the hillcrest through time

for $\tau_d = 1$ are shown in Figure 8g and 8h. Changes in the relaxation time of the hillcrest due to lofting processes can be found by subtracting the lines in Figures 8g and 8h from the lines in Figure 8e and 8f. The difference in these trends demonstrates that lofting process can have a significant effect on the transient behavior of the hillslope.

[37] Figure 9 shows dimensionless hillcrest offset distances for runs with different values of θ_Z and $\hat{t}_{kpd}$. These curves show that the trend in faster response times (lower κ values) for lower values of θ_Z shortly after the passage of the knickpoint dominates the behavior of the hillcrest. Specifically, for lower values of θ_Z the initial response of the hillcrest to perturbations is faster than for lower values of θ_Z, and most of the divides motion occurs in these early stages. Recall that lower values of θ_Z would result from shorter hillslopes, lower background incision rates, greater diffusivities, and greater soil production length scales.

4.1.2. Linear-Critical Flux Law

[38] When hillslope sediment transport follows the linear-critical sediment flux law (equation 8), we define θ_{kp} to be the ratio of the height of the knickpoints to $\hat{Z}_{ls}$. Unlike the linear case, linear-critical hillslopes with the same value of θ_Z do not lead to identical hillcrest migration behavior if τ_d and θ_{kp} are the same. Because we do not have an analytical solution for the maximum offset distance as a function of the other model parameters, using equation (40) to calculate the decay rates is difficult because the final state of the hillcrest may only be calculated by iterative numerical means. We have chosen instead to directly compare the motion of the hillcrest for various parameter values (Figure 10). For low-relief slopes, the behavior of hillslopes with linear-critical sediment transport approximates the behavior of slopes with linear sediment transport for reasons discussed in section 3.1. As the relief increases, however, the nonlinear flux terms begin to dominate transport [*Roering et al.*, 2001], and the behavior of the hillcrest departs from the behavior of hillslopes with a linear sediment flux law.

[39] Figure 10a compares the migration of the hillcrest for linear-critical slopes with varying dimensionless relief but identical values of θ_Z. As the relief increases, the distance that the hillcrest migrates also increases. Although the hillcrest migrates further for the hillslopes with higher relief, the adjustment rate is faster such that they spend less time out of the symmetry after the second knickpoint has migrated past the base of the hillslope (Figure 10a). If the relief is held constant, varying the knickpoint ratio θ_{kp} affects the distance the hillcrest travels but has only a negligible effect on how long the hillcrest spends away from $\hat{x} = 1$ after the passage of the second knickpoint (Figure 10b). This implies that the adjustment rate for hillslopes with variations in θ_{kp} is approximately the same during the restore phase, a result that mirrors the behavior of the linear case (see Figure 8b). Similarly, the response of the hillcrest mirrors the linear case for variations in θ_Z (Figure 10c) and τ_d (Figure 10d). As noted in section 4.1.1., the richest variation in the behavior of the hillcrest occurs when θ_Z is varied. Variations in the dimensionless relief, the density ratio, and the knickpoint ratio lead to systematic variations in the response rate in that varying these parameters will either increase or decrease the response rate in the same manner regardless of the knickpoint delay.
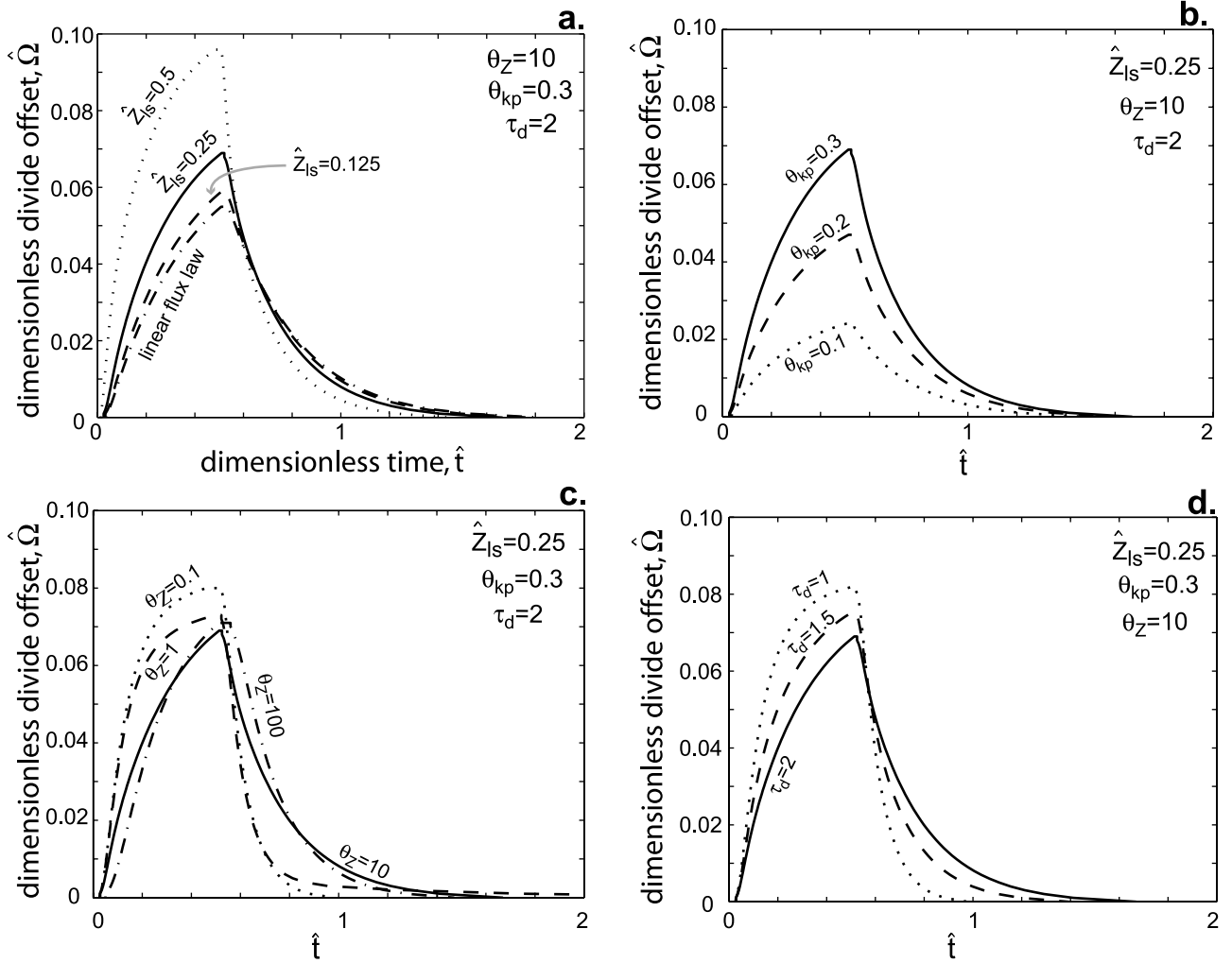
Figure 10. Hillcrest offset as a function of dimensionless time. All runs use a linear-critical sediment flux law except where labeled. The knickpoint delay ($\hat{t}_{kpd}$) is 0.5. (a) Variations in $\hat{Z}_{ls}$. (b) Variations in θ_{kp}. (c) Variations in θ_Z. (d) Variations in τ_d. The solid line in Figures 10a–10d is from the same model run.

4.1.3. Soil Storage and Thickness Effects

[40] To track soil storage, we measure the ratio of the total storage of sediment on the hillslope at dimensionless time $\hat{t}$ to the total soil storage at steady state. We name this ratio the soil storage ratio θ_{ss}. For both flux laws, the soil thickness, $\hat{h}$, reacts more slowly than the surface topography (Figure 7b) such that when the hillcrest returns to the symmetric position at $\hat{x} = 1$, the soil has not returned to a steady state (where $\partial\hat{h}/\partial\hat{t} = 0$ and $\theta_{ss} = 1$). Typical plots of the time evolution of soil storage after perturbations by knickpoints are shown in Figure 11. The lines in Figure 11 end when the hillcrest in the simulation has returned to the equilibrium position at $\hat{x} = 1$. The reduction in soil storage on the hillslopes caused by the evacuation of sediment due to the knickpoints will be greater for increasing τ_d and θ_{kp}. Hillslopes with faster background incision rates $\hat{I}$ have smaller changes in soil storage on the hillslope because slower incision rates lead to thicker soils, and the amount of sediment evacuated from the hillslope will be a smaller percentage of the total soil storage in thicker soils. We restrict our description of the dynamic behavior of soil
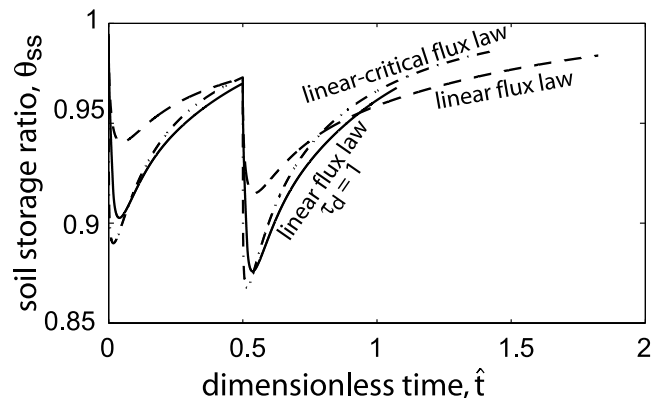

Figure 11. Change in soil storage ratio through time. All runs have $\theta_Z = 10$, $\hat{t}_{kpd} = 0.5$, and $\theta_{kp} = 0.3$. All runs have $\tau_d = 2$ unless noted. Hillslope with linear-critical flux law has a $\hat{Z}_{ls}$ value of 0.5.
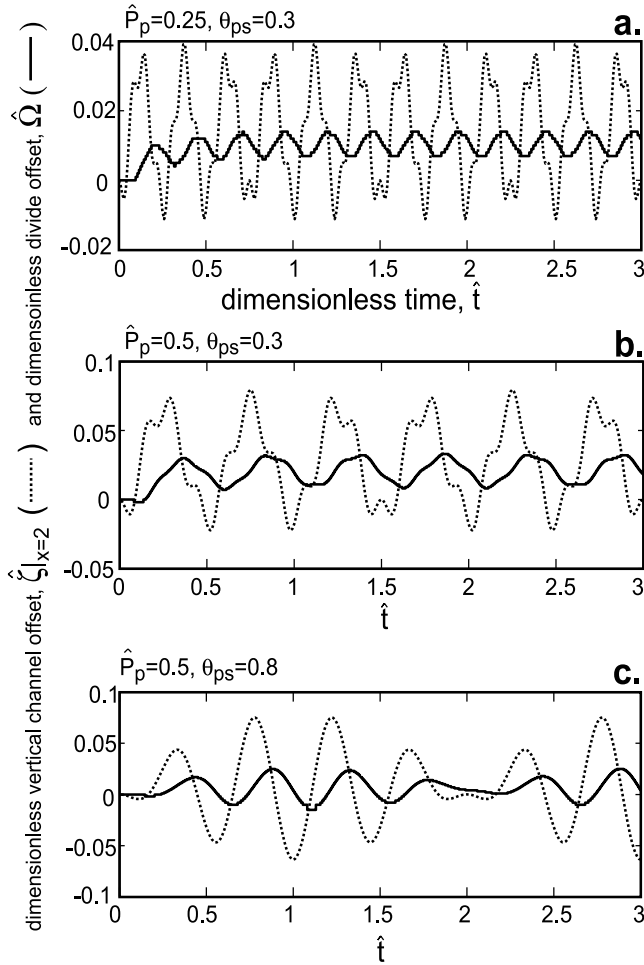
Figure 12. Vertical channel offset and hillcrest offset for hillslopes bounded by channels with oscillating incision rates. All runs use a linear-critical flux law and have $\theta_Z = 10$, $\tau_d = 2$, $\hat{Z}_{ls} = 0.5$, $\hat{I}_{avg} = -0.2$, $\hat{A}_p = 0.2$, and $\theta_A = 1$. The dotted lines are the vertical channel offset, and the solid lines are the hillcrest offset. The $\hat{P}_p$ and θ_P values are listed above each plot.

storage following perturbation to this simple summary, as a detailed analysis is beyond the scope of this contribution.

4.2. Effect of Variations in Amplitude and Frequency of Incision Rates

[41] The incision rate of a channel is related to water discharge and sediment flux [e.g., *Howard et al.*, 1994; *Sklar and Dietrich*, 2004; *Whipple and Tucker*, 1999], both of which are likely to be stochastic in time [e.g., *Snyder et al.*, 2003; *Tucker*, 2004]. The probability distribution of discharge and sediment flux will vary depending on the size of the basin, so, for example, if two adjacent basins are of different size and are eroding at the same rate averaged over a time far greater than the time of individual events, one basin may be incising with frequent but low-magnitude incision events while the other may be incising in infrequent but high-magnitude events. This discrepancy in the frequency and magnitude of incision events in adjacent basins with the same long-term lowering rate can perturb the location of the hillcrest separating these basins.

[42] Here we approximate the time varying nature of stream incision by modeling the incision rate in the primary and secondary channels with sine waves of different amplitudes and frequencies. We make this simplification because the computational time required to run the large number of simulations that would need to be performed to quantify hillcrest migration based on a stochastic distribution is prohibitive. The approach of modeling erosion rate variability using sinusoidal functions has been taken by *Furbish and Fagherazzi* [2001] in investigating the transient response of a hillslope with a fixed hillcrest and a linear sediment flux law. Here we expand this analysis to investigate the behavior of the hillcrest as the two channels incise with the same average incision rate but with different frequencies and amplitudes.

[43] We model adjacent channels that, on a long-term average, incise at the same rate $\hat{I}_{avg}$. The incision rate of the primary channel has a dimensionless amplitude $\hat{A}_p$ and a dimensionless period $\hat{P}_p$ such that the incision rate of the primary channel ($\hat{I}_p$) through time is:

$$\hat{I}_p = \hat{I}_{avg} - \hat{A}_p \sin\left(\frac{2\pi}{\hat{P}_p}\hat{t}\right). \tag{42}$$

All dimensionless amplitudes and incision rates are scaled analogously to $\hat{I}$ (see equation (13)) and all dimensionless periods are scaled analogously to dimensionless time (see equation (15)). The incision in the secondary channel has an amplitude and period that are related to the amplitude and period of the primary channel by

$$\hat{A}_s = \theta_A \hat{A}_p, \tag{43a}$$

$$\hat{P}_s = \theta_P \hat{P}_p. \tag{43b}$$

We call θ_A and θ_P the amplitude and period ratios, respectively. The downcutting rate of the secondary channel is then

$$\hat{I}_s = \hat{I}_{avg} - \theta_A \hat{A}_p \sin\left(\frac{2\pi}{\theta_P \hat{P}_p}\hat{t}\right). \tag{44}$$

[44] We present here a general overview of the behavior of the hillslopes and hillcrests subject to sinusoidal variations in the downcutting rates of the bordering channels, rather than perform a complete study of parameter space. Our numerical experiments focus on hillslopes on which sediment transport can be described by the linear-critical sediment flux law. We illustrate typical behavior of the hillcrest for hillslopes where $\theta_Z = 10$, $\hat{Z}_{ls} = 0.5$ (this means the relief of the linear-critical hillslope will be ~0.4 because the linear-critical flux law limits the steepness of the hillslope gradient on high-relief hillslopes), and $\tau_d = 2$. From the results in section 4.1.2., it should be noted that the hillcrest will move greater distances than the runs presented here if τ_d were reduced, and the hillcrest would move more slowly and move a shorter distance if $\hat{Z}_{ls}$ were decreased.

[45] If the two channels have different instantaneous incision rates (e.g., θ_A and θ_p are not equal to one), vertical
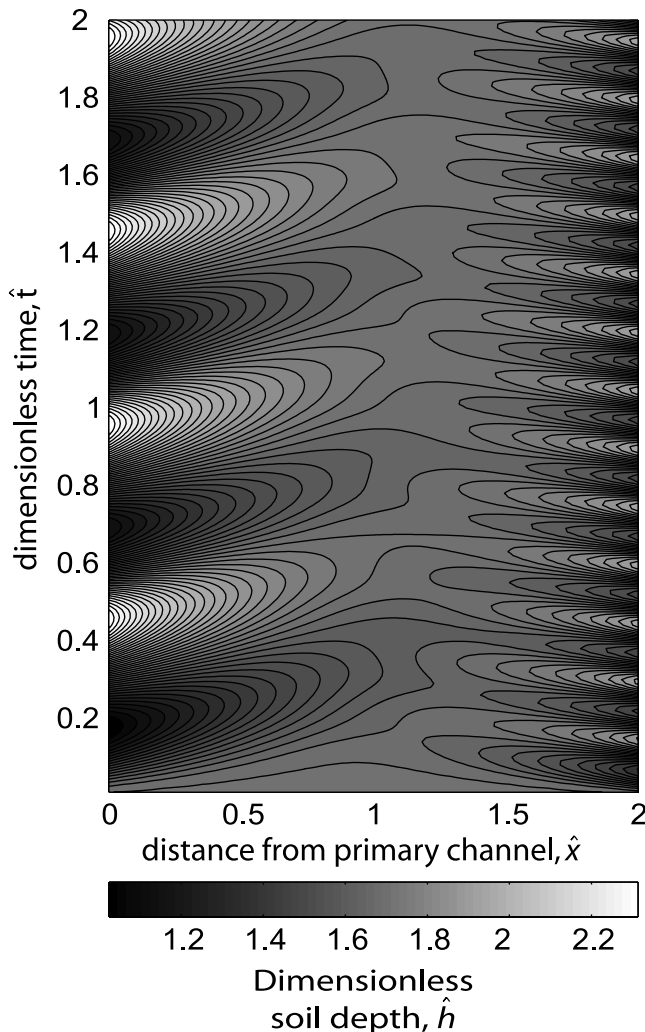
Figure 13. Soil thickness as a function of time and space for a hillslope bounded by channels with oscillating incision rates. A linear-critical flux law is used. Parameter values are $\theta_Z = 10$, $\tau_d = 2$, $\hat{Z}_{ls} = 0.5$, $\hat{I}_{avg} = -0.2$, $\hat{A}_p = 0.2$, and $\theta_A = 1$, $\hat{P}_p = 0.5$, and $\theta_P = 0.3$.

channel offsets will be generated though time. Greater channel offsets will lead to greater distances of hillcrest migration. The migration of the hillcrest is similar to the temporal pattern of channel offset, but the oscillation of the hillcrest will be damped and shifted in phase compared to the oscillations in the vertical channel offset. The phase shift is significant because it means that when vertical channel offsets are nil, the divide will still be offset.

[46] *Furbish and Fagherazzi* [2001] found that higher-frequency oscillations (e.g., lower values of $\hat{P}_p$, more cycles of the incision rate in a given time period) in the channel incision rate are less likely to reach the drainage hillcrest than lower-frequency oscillations (e.g., higher values of $\hat{P}_p$, fewer cycles of the incision rate in a given time period). We find this to be true in the case where the hillcrest is free to migrate and break the symmetry of the hillslope. The average offset over time may be solved analytically; this average offset will increase linearly with $\hat{A}_p$, increase monotonically with θ_A and $\hat{P}_p$, and decrease monotonically with θ_p.

[47] Three examples of vertical channel offsets and hillcrest offsets as a function of time are plotted in Figures 12a, 12b, and 12c. The high-frequency oscillations in Figure 12a result in smaller hillcrest offsets than the lower-frequency examples of Figures 12b and 12c. The oscillations in the incision rate of the bounding channels will lead to oscillations in the vertical channel offset, and higher-frequency oscillations in the vertical offset will be less likely to influence the migration of the hillcrest than lower-frequency oscillations. Figure 12 demonstrates that the response of the hillcrest reflects the vertical channel offset, but this signal is damped and delayed. We point out that the dimensionless time $\hat{t}$ is scaled by the diffusive timescale T_D, which ranges from 10^4 to 10^6 years [*Mudd and Furbish*, 2004]. Variations in downcutting on the human timescale (e.g., a 10 year cycle of incision rates caused by, for example, El Nino climate cycles, gives a $\hat{P}_p$ of 10^{-5} for a 100 m long hillslope with a diffusivity of 0.01 m^2 yr^{-1}) will likely not be reflected in the hillcrest, whereas variations caused by long-term climate change will be reflected in the motion of the hillcrest. In Figures 12a and 12b, all parameters are the same except for the periods of the incision rate fluctuations. Note that in Figure 12a, which has a shorter period (lower $\hat{P}_p$), the hillcrest offset is a smaller fraction of the channel offset than in the case of Figure 12b.

[48] Consider a dimensional realization of Figure 12 where the hillslope has a length of 20 m and a diffusivity of 0.01 m^2 yr^{-1}. This gives a T_D value of 40 ka. The relief of the hillslope is ~8 m. In the case of Figure 13a, where $\hat{P}_p = 0.25$, the incision rate of the primary channel varies over a period of 10 ka, whereas the secondary channel varies over a period of 3 ka ($\theta_p = 0.3$). These periods change to 20 ka and 6.67 ka for the hillslope modeled in Figure 12b ($\hat{P}_p = 0.5$, $\theta_p = 0.3$). In both these cases, the hillcrest will migrate with a period that is approximately the period of the primary (low frequency) channel (10 and 20 ka for Figures 12a and 12b, respectively). Dimensional vertical offsets between the two channels would be 0.8 m in the case of Figure 12a and 1.6 m, in the case of Figure 12b. The maximum hillcrest offsets would be 0.28 m for the case of Figure 12a and 0.66 m for the case of Figure 12b.

[49] The damping of high-frequency variations is also reflected in the soil storage and soil thickness. Figure 13 shows the spatial variation in soil thickness as a function of time. The secondary channel has higher-frequency oscillations; these oscillations in soil thickness are not transmitted from the secondary channel to the hillcrest, rather the soil thickness at the hillcrest is dominated by the signal from the primary channel with a lower frequency of oscillation. In summary, the transient behavior of the surface topography, the location of the hillcrest, and the soil thickness will be dominated by channels whose incision rate varies with low frequency.

5. Conclusions

[50] We have investigated the behavior of lateral hillcrest offset and migration under conditions of vertical offsets in the elevation of channels bounding a hillcrest and locally varying incision rates in the bounding channels. For hillslopes on which sediment transport takes on specific transport relations (linear or linear-critical flux laws), the offset

from symmetry of the hillcrest is a geometric function of the vertical channel offset. The transient response of the hillcrest is faster for knickpoints with greater relief (larger θ_{kp}, the ratio between the relief of the knickpoint and the relief of the hillslope) and slower for increasing density ratios on the hillslope (the ratio of the dry bulk density of the rock to the dry bulk density of the soil, τ_d). The rate of hillcrest migration is sensitive to the ratio between the diffusive timescale of the hillslope and the time it takes to erode through a fixed thickness of soil (2γ) at the background incision rate; we name this ratio θ_Z. Although the response rate of the hillcrest varies in time, most of the divide migration take place early after disturbance of a channel; the divide will migrate faster for lower values of θ_Z. All else being equal, shorter hillslopes, lower background incision rates, greater diffusivities, and greater soil production length scales will lead to faster hillcrest migration. Within a reasonable range of parameter values (e.g., $\theta_Z = 1-100$, $\tau_d = 1-2$, $\theta_{kp} = 0.1-0.3$), the divide offset will reach a significant portion (e.g., $\exp[-1]$) of its theoretical maximum offset within a fraction (e.g., <0.5) of the diffusive timescale ($T_D = \lambda^2/D$) of the hillslope. For hillslopes where sediment transport follows a linear-critical flux law, increasing hillslope relief will also lead to faster responses of the hillcrest to channel perturbations.

[51] The hillcrests of hillslopes that are bounded by channels whose incision rates vary in time migrate in a manner that reflects the vertical channel offset generated by the transient channel downcutting rates. Higher-frequency oscillations in the channel downcutting rate are less likely to influence the position of the hillcrest than low-frequency oscillations. While we have not performed an exhaustive study of the effect of incision rate oscillations, we have found that for incision rates that vary periodically over a time that is less than one quarter of the diffusive timescale ($T_D = \lambda^2/D$, for typical hillslopes $T_D = 10^3-10^7$ years), the migration of the hillcrest in our simulations was less than 2% of the hillslope length. If the incision rates of the two channels bounding a hillslope are periodic through time, then the horizontal offset of the hillcrest is also periodic in time. The oscillation of the hillcrest will be out of phase with the oscillation of the vertical offset of the channels, and we have found that the hillcrest can be in an asymmetric position when there is no difference in the elevation in the channels. If channels bounding a hillcrest are at the same elevation, but the hillcrest is not equidistant from the two channels, the this could be a indication of an imbalance in the erosion rates of the two channels bounding the hillslope.

[52] We have focused primarily on situations in which the long-term average incision rates in the two channels are the same. This situation leads to hillcrests that oscillate about a central location, but we do not invoke a feedback that can fix a hillcrest in a new location after a transient disturbance in the channel downcutting rates or permanently change the spatial distribution of the hillcrests. The presence of features such as stream capture in the field and the experiments of *Hasbargen and Paola* [2000] indicate that there may be positive feedbacks between divide migration, channel offsets, and local incision rates. It is generally agreed that the longitudinal profiles and incision rates of fluvial channels are nonlinearly related to both drainage area and sediment supply [e.g., *Sklar and Dietrich*, 2004; *Whipple*, 2004]. A migrating divide will change both the drainage area and sediment supply to the two channels bounding it. If a transient change in channel downcutting persists long enough and is great enough to change the drainage area or sediment supply in a manner that affects the incision rate and profile of the channel, the position of the hillcrest may become "fixed" such that the hillcrest does not move back to its original position, and the drainage basin configuration may change to reflect a new equilibrium configuration.

Notation

$\hat{A}_p, \hat{A}_s$ amplitude of the incision rate in the primary and secondary channel, respectively (dimensionless).

D sediment diffusivity ($L^2 T^{-1}$).

η elevation of soil bedrock boundary (L).

η_0 elevation of soil-bedrock boundary at $x = 0$ (L).

η_{bl} elevation of soil-bedrock boundary relative to base level (L).

$\hat{\eta}$ dimensionless elevation of soil-bedrock boundary relative to base level.

ϕ dimensionless function of slope that varies with the sediment flux law.

γ soil production decay length scale (L).

$h, \hat{h}$ soil thickness (L) and dimensionless soil thickness, respectively.

$I, \hat{I}$ dimensional ($L T^{-1}$) and dimensionless incision rate, respectively.

$\hat{I}_p$ incision rate of secondary channel (dimensionless).

$\hat{I}_s$ incision rate of primary channel (dimensionless).

$\hat{I}_{avg}$ long-term average incision rate(dimensionless).

K sediment dispersion coefficient ($M L^{-1} T^{-1}$).

κ_p decay coefficient for the push phase of hillcrest migration (dimensionless).

κ_r decay coefficient for the restore phase of hillcrest migration (dimensionless).

λ length of the hillslope (half the distance between channels) (L).

$\hat{\Omega}$ dimensionless hillcrest offset.

$\hat{\Omega}_{lr}, \hat{\Omega}_{cs}$ dimensionless hillcrest offset of a low-relief and critical slope hillslope, respectively.

p_η soil production rate ($L T^{-1}$).

$\hat{P}_p, \hat{P}_s$ period of the variation in incision rate in the primary and secondary channel, respectively (dimensionless).

$\bar{\rho}_s$ depth-averaged dry bulk density of hillslope soil ($M L^{-3}$).

ρ_η dry bulk density of parent material ($M L^{-3}$).

S_c critical slope for linear-critical flux law (dimensionless).

S_T threshold slope (dimensionless).

θ_L length ratio (dimensionless).

θ_t time ratio (dimensionless).

θ_{kp} knickpoint ratio (dimensionless).

θ_I incision ratio (dimensionless).

θ_O offset ratio (dimensionless).

θ_A amplitude ratio (dimensionless).

θ_P period ratio (dimensionless).

θ_{ss} soil storage ratio (dimensionless).

θ_Z — ratio of erosion timescale to diffusive timescale (dimensionless).

τ_d — density ratio (dimensionless).

$t, \hat{t}$ — dimensional (T) and dimensionless time.

$\hat{t}_{sc}$ — dimensionless time to stream capture.

$\hat{t}_{kpd}$ — dimensionless time of knickpoint delay.

T_p — production timescale (T).

T_D — diffusive (or relaxation) timescale (T).

$\hat{u}_d$ — Dimensionless velocity of the hillcrest.

$\bar{v}_x$ — depth-averaged sediment velocity in the x direction (L T^{-1}).

W_0 — nominal rate of soil production (L T^{-1}).

$x, \hat{x}$ — dimensional (L) and dimensionless distance from the primary channel.

$\hat{x}_d$ — dimensionless location of the hillcrest.

$\hat{Z}$ — dimensionless elevation of the hillcrest.

$\hat{Z}_{ls}$ — dimensionless elevation of the hillcrest for a symmetric hillslope with a linear sediment flux law.

ζ — elevation of soil-bedrock boundary (L).

ζ_0 — elevation of soil-bedrock boundary at $x = 0$ (L).

ζ_{bl} — elevation of soil-bedrock boundary relative to base level (L).

$\hat{\zeta}$ — dimensionless elevation of soil-bedrock boundary relative to base level.

References

Anderson, R. S. (2002), Modeling the tor-dotted crests, bedrock edges, and parabolic profiles of high alpine surfaces of the Wind River Range, Wyoming, *Geomorphology*, 46(1–2), 35–58.

Andrews, D. J., and R. C. Bucknam (1987), Fitting degradation of shoreline scarps by a nonlinear diffusion-model, *J. Geophys. Res.*, 92(B12), 12,857–12,867.

Benda, L., and T. Dunne (1997), Stochastic forcing of sediment routing and storage in channel networks, *Water Resour. Res.*, 33(12), 2865–2880.

Bishop, P., R. W. Young, and I. Mcdougall (1985), Steam profile change and longterm landscape evolution—Early Miocene and modern rivers of the East Australian Highland Crest, central New-South-Wales, Australia, *J. Geol.*, 93(4), 455–474.

Bras, R. L., G. E. Tucker, and V. Teles (2003), Six myths about mathematical modeling in geomorphology, in *Prediction in Geomorphology*, *Geophys. Monogr. Ser.*, vol. 135, edited by P. R. Wilcock and R. M. Iverson, pp. 63–79, AGU, Washington, D. C.

Brimhall, G. H., O. A. Chadwick, C. J. Lewis, W. Compston, I. S. Williams, K. J. Danti, W. E. Dietrich, M. E. Power, D. Hendricks, and J. Bratt (1992), Deformational mass-transport and invasive processes in soil evolution, *Science*, 255(5045), 695–702.

Burbank, D. W., J. Leland, E. Fielding, R. S. Anderson, N. Brozoic, M. R. Reid, and C. Duncan (1996), Bedrock incision, rock uplift and threshold hillslopes in the northwestern Himalayas, *Nature*, 379(8), 505–510.

Chen, Y. G., W. S. Chen, Y. Wang, P. W. Lo, T. K. Liu, and J. C. Lee (2002), Geomorphic evidence for prior earthquakes: Lessons from the 1999 Chichi earthquake in central Taiwan, *Geology*, 30(2), 171–174.

Crosby, B. T., and K. X. Whipple (2005), Knickpoint initiation and distribution within fluvial networks: 236 waterfalls in the Waipaoa River, North Island, New Zealand, *Geomorphology*, in press.

Culling, W. E. H. (1963), Soil creep and the development of hillside slopes, *J. Geol.*, 71(2), 127–161.

Densmore, A. L., M. A. Ellis, and R. S. Anderson (1998), Landsliding and the evolution of fault bounded mountains, *J. Geophys. Res.*, 103, 15,203–15,219.

Dietrich, W. E., D. G. Bellugi, L. S. Sklar, and J. D. Stock (2003), Geomorphic transport laws for predicting landscape form and dynamics, in *Prediction in Geomorphology*, *Geophys. Monogr. Ser.*, vol. 135, edited by P. R. Wilcock and R. M. Iverson, pp. 103–132, AGU, Washington, D. C.

Fernandes, N. F., and W. E. Dietrich (1997), Hillslope evolution by diffusive processes: The timescale for equilibrium adjustments, *Water Resour. Res.*, 33(6), 1307–1318.

Finlayson, D. P., D. R. Montgomery, and B. Hallet (2002), Spatial coincidence of rapid inferred erosion with young metamorphic massifs in the Himalayas, *Geology*, 30(3), 219–222.

Furbish, D. J., and S. Fagherazzi (2001), Stability of creeping soil and implications for hillslope evolution, *Water Resour. Res.*, 37(10), 2607–2618.

Gabet, E. J. (2000), Gopher bioturbation: Field evidence for non-linear hillslope diffusion, *Earth Surf. Processes Landforms*, 25(13), 1419–1428.

Gabet, E. J., O. J. Reichman, and E. W. Seabloom (2003), The effects of bioturbation on soil processes and sediment transport, *Annu. Rev. Earth Planet. Sci.*, 31, 249–273.

Gilbert, G. K. (1877), *Report on the Geology of the Henry Mountains*, 160 pp., U.S. Gov. Print. Off., Washington, D. C.

Hack, J. T. (1960), Interpretation of erosional topography in humid temperate region, *Am. J. Sci.*, 258-A, 80–97.

Harbor, D. J. (1997), Landscape evolution at the margin of the Basin and Range, *Geology*, 25(12), 1111–1114.

Hasbargen, L. E., and C. Paola (2000), Landscape instability in an experimental drainage basin, *Geology*, 28(12), 1067–1070.

Heimsath, A. M., W. E. Dietrich, K. Nishiizumi, and R. C. Finkel (1999), Cosmogenic nuclides, topography, and the spatial variation of soil depth, *Geomorphology*, 27(1-2), 151–172.

Heimsath, A. M., J. Chappell, W. E. Dietrich, K. Nishiizumi, and R. C. Finkel (2000), Soil production on a retreating escarpment in southeastern Australia, *Geology*, 28(9), 787–790.

Heimsath, A. M., J. Chappell, W. E. Dietrich, K. Nishiizumi, and R. C. Finkel (2001), Late Quaternary erosion in southeastern Australia: A field example using cosmogenic nuclides, *Quat. Int.*, 83–85, 169–185.

Heimsath, A. M., J. Chappell, N. A. Spooner, and D. G. Questiaux (2002), Creeping soil, *Geology*, 30(2), 111–114.

Howard, A. D. (1988), Equilibrium models in geomorphology, in *Modeling in Geomorphic Systems*, edited by M. G. Anderson, pp. 49–72, John Wiley, Hoboken, N. J.

Howard, A. D. (1994), A detachment-limited model of drainage-basin evolution, *Water Resour. Res.*, 30(7), 2261–2285.

Howard, A. D., W. E. Dietrich, and M. A. Siedl (1994), Modeling fluvial erosion on regional to continental scales, *J. Geophys. Res.*, 99, 13,971–13,986.

Jyotsna, R., and P. K. Haff (1997), Microtopography as an indicator of modern hillslope diffusivity in arid terrain, *Geology*, 25(8), 695–698.

Kirchner, J. W., R. C. Finkel, C. S. Riebe, D. E. Granger, J. L. Clayton, J. G. King, and W. F. Megahan (2001), Mountain erosion over 10 yr, 10 k.y., and 10 m.y. time scales, *Geology*, 29(7), 591–594.

Kirkby, M. J. (1967), Measurement and theory of soil creep, *J. Geol.*, 75(4), 359–378.

Kobor, J. S., and J. J. Roering (2004), Systematic variation of bedrock channel gradients in the central Oregon Coast Range: Implications for rock uplift and shallow landsliding, *Geomorphology*, 62(3-4), 239–256.

Mather, A. E., A. M. Harvey, and M. Stokes (2000), Quantifying long-term catchment changes of alluvial fan systems, *Geol. Soc. Am. Bull.*, 112(12), 1825–1833.

Matmon, A., P. R. Bierman, J. Larsen, S. Southworth, M. Pavich, R. Finkel, and M. Caffee (2003), Erosion of an ancient mountain range, the Great Smoky Mountains, North Carolina and Tennessee, *Am. J. Sci.*, 303(9), 817–855.

McKean, J. A., W. E. Dietrich, R. C. Finkel, J. R. Southon, and M. W. Caffee (1993), Quantification of soil production and downslope creep rates from cosmogenic Be-10 accumulations on a hillslope profile, *Geology*, 21(4), 343–346.

Meigs, A., N. Brozovic, and M. L. Johnson (1999), Steady, balanced rates of uplift and erosion of the Santa Monica Mountains, California, *Basin Res.*, 11(1), 59–73.

Meyerhof, H. A. (1972), Postorogenic development of Appalachians, *Geol. Soc. Am. Bull.*, 83(6), 1709–1727.

Mudd, S. M., and D. J. Furbish (2004), The influence of chemical denudation on hillslope morphology, *J. Geophys. Res.*, 109, F02001, doi:10.1029/2003JF000087.

Pelletier, J. D. (2004), Persistent drainage migration in a numerical landscape evolution model, *Geophys. Res. Lett.*, 31, L20501, doi:10.1029/2004GL020802.

Reneau, S. L., and W. E. Dietrich (1991), Erosion rates in the southern Oregon Coast Range—Evidence for an equilibrium between hillslope erosion and sediment yield, *Earth Surf. Processes Landforms*, 16(4), 307–322.

Riebe, C. S., J. W. Kirchner, D. E. Granger, and R. C. Finkel (2000), Erosional equilibrium and disequilibrium in the Sierra Nevada, inferred from cosmogenic Al-26 and Be-10 in alluvial sediment, *Geology*, *28*(9), 803–806.

Roering, J. J., P. Almond, P. Tonkin, and J. McKean (2002), Soil transport driven by biological processes over millennial time scales, *Geology*, *30*(12), 1115–1118.

Roering, J. J., J. W. Kirchner, and W. E. Dietrich (1999), Evidence for nonlinear, diffusive sediment transport on hillslopes and implications for landscape morphology, *Water Resour. Res.*, *35*(3), 853–870.

Roering, J. J., J. W. Kirchner, and W. E. Dietrich (2001), Hillslope evolution by nonlinear, slope-dependent transport: Steady state morphology and equilibrium adjustment timescales, *J. Geophys. Res.*, *106*(B8), 16,499–16,513.

Sklar, L. S., and W. E. Dietrich (2004), A mechanistic model for river incision into bedrock by saltating bed load, *Water Resour. Res.*, *40*, W06301, doi:10.1029/2003WR002496.

Small, E. E., R. S. Anderson, and G. S. Hancock (1999), Estimates of the rate of regolith production using Be-10 and Al-26 from an alpine hill-slope, *Geomorphology*, *27*(1-2), 131–150.

Smith, T. R., and F. P. Bretherton (1972), Stability and the conservation of mass in drainage basin evolution, *Water Resour. Res.*, *8*(6), 1506–1528.

Snyder, N. P., K. X. Whipple, G. E. Tucker, and D. J. Merritts (2003), Importance of a stochastic distribution of floods and erosion thresholds in the bedrock river incision problem, *J. Geophys. Res.*, *108*(B2), 2117, doi:10.1029/2001JB001655.

Tucker, G. E. (2004), Drainage basin sensitivity to tectonic and climatic forcing: Implications of a stochastic model for the role of entrainment and erosion thresholds, *Earth Surf. Processes Landforms*, *29*, 185–205.

Tucker, G. E., and R. L. Bras (1998), Hillslope processes, drainage density, and landscape morphology, *Water Resour. Res.*, *34*(10), 2751–2764.

van der Beek, P., M. A. Summerfield, J. Braun, R. W. Brown, and A. Fleming (2002), Modeling postbreakup landscape development and denudational history across the southeast African (Drakensberg Escarpment) margin, *J. Geophys. Res.*, *107*(B12), 2351, doi:10.1029/2001JB000744.

Whipple, K. X. (2004), Bedrock rivers and the geomorphology of active orogens, *Annu. Rev. Earth Planet. Sci.*, *32*, 151–185.

Whipple, K. X., and G. E. Tucker (1999), Dynamics of the stream-power river incision model: Implications for height limits of mountain ranges, landscape response timescales, and research needs, *J. Geophys. Res.*, *104*(B8), 17,661–17,674.

Willgoose, G., R. L. Bras, and I. Rodriguez-Iturbe (1991), A coupled channel network growth and hillslope evolution model: 1. Theory, *Water Resour. Res.*, *27*(7), 1671–1684.

Young, A. (1978), A twelve-year record of soil movement on a slope, *Z. Geomorph. Suppl.*, *29*, 104–110.

Young, R., and I. McDougall (1993), Long-term landscape evolution— Early Miocene and modern rivers in southern New South Wales, Australia, *J. Geol.*, *101*(1), 35–49.

Zaprowski, B. J., E. B. Evenson, F. J. Pazzaglia, and J. B. Epstein (2001), Knickzone propagation in the Black Hills and northern High Plains: A different perspective on the late Cenozoic exhumation of the Laramide Rocky Mountains, *Geology*, *29*(6), 547–550.

————————————

D. J. Furbish, Department of Earth and Environmental Sciences, Vanderbilt University, Nashville, TN 37235, USA.

S. M. Mudd, Department of Civil and Environmental Engineering, Vanderbilt University, Nashville, VU Station B 351831, 2301 Vanderbilt Place, TN 37235, USA. (simon.m.mudd@vanderbilt.edu)